

## The Atmospheric Oxidizing Capacity in China: Part 2. Sensitivity to emissions of primary pollutants

5

Jianing Dai<sup>a</sup>, Guy P. Brasseur<sup>a,e,f</sup>, Mihalis Vrekoussis<sup>b,g,h</sup>, Maria Kanakidou<sup>b,d</sup>, Kun Qu<sup>b</sup>,  
Yijuan Zhang<sup>b</sup>, Hongliang Zhang<sup>c</sup>, Tao Wang<sup>f</sup>

10 <sup>a</sup> Environmental Modelling Group, Max Planck Institute for Meteorology, Hamburg, 20146,  
Germany

<sup>b</sup> Institute of Environmental Physics (IUP), University of Bremen, Bremen, 28359, Germany

<sup>c</sup> Department of Environmental Science and Engineering, Fudan University, Shanghai, 200433,  
China

15 <sup>d</sup> Environmental Chemical Processes Laboratory, Department of Chemistry, University of  
Crete, Heraklion, 70013, Greece

<sup>e</sup> National Center for Atmospheric Research, Boulder, Colorado, 80307, USA

<sup>f</sup> Department of Civil and Environmental Engineering, The Hong Kong Polytechnic University,  
Hong Kong, China

20 <sup>g</sup> Center of Marine Environmental Sciences (MARUM), University of Bremen, Bremen,  
28359, Germany

<sup>h</sup> Climate and Atmosphere Research Center (CARE-C), The Cyprus Institute, Nicosia, Cyprus

*Correspondence to:* Guy P. Brasseur (guy.brasseur@mpimet.mpg.de)

25

30

35

40

## Abstract

45 The Atmospheric Oxidation Capacity (AOC), often referred to as the self-cleansing ability of  
the atmosphere, considerably affects the concentrations of photochemical air pollutants.  
Despite substantial reductions in anthropogenic emissions of key chemical compounds in  
China, the mechanisms that determine the changes in the atmospheric oxidation capacity are  
50 still not sufficiently understood. Here, a regional chemical transport model is employed to  
quantify the sensitivity of air pollutants and photochemical parameters to specified emission  
reductions for winter and summer conditions (January and July 2018). The model simulations  
show that, in winter, a 50% decrease in nitrogen oxide (NO<sub>x</sub>) emissions leads to an increase of  
6–12 ppbv (15–33%) in surface ozone (O<sub>3</sub>) concentrations across China. In summer, the O<sub>3</sub>  
concentration decreases by 2–8 ppbv (3–12%) in NO<sub>x</sub>-limited areas, while it increases by up to  
55 8 ppbv (17%) in volatile organic compounds (VOCs)-limited areas. This O<sub>3</sub> increase is  
associated with a reduced NO<sub>x</sub> titration effect and with higher levels of hydroxyl (OH) and  
hydroperoxyl (HO<sub>2</sub>) radicals due to a reduced loss by reactions with nitrogen dioxide (NO<sub>2</sub>)  
and by a decreased aerosol uptake. With an additional 50% reduction in anthropogenic VOCs  
emissions, the O<sub>3</sub> concentration decreases by 5–12 ppbv (6–15%) in the entire geographic area,  
60 with an exception in the regions, where the role of BVOCs is crucial to ozone formation.  
Further, the adopted reduction in NO<sub>x</sub> emission leads to an increase of AOC by 18% in VOC-  
limited areas. This specific increase is associated with the enhanced radical cycles from the  
photolysis of oxidized VOCs (OVOCs) and the oxidation of alkenes by OH radicals and O<sub>3</sub>.  
This study highlights that the photolysis of OVOCs and the oxidation of alkenes and aromatic  
65 compounds in urban areas promote an increase in O<sub>3</sub> when the NO<sub>x</sub> emissions are reduced. To  
mitigate O<sub>3</sub> rises in urban areas, a joint reduction in the emission of NO<sub>x</sub> and in specific VOCs  
species, including alkenes, aromatics, and unsaturated OVOCs, including methanol and  
ethanol, should be implemented.

Despite substantial reductions in anthropogenic emissions, ozone (O<sub>3</sub>) pollution remains a  
70 severe environmental problem in urban areas of China. The reduction in the emission of  
pollutants affects formation of ozone through the changes in concentrations of O<sub>3</sub> precursors  
and intermediates species as well as in the oxidation capacity of the atmosphere. However, the  
underlying mechanisms driving O<sub>3</sub> changes are still not fully understood. Here, we employ a  
regional chemical transport model to quantify the changes in the formation of ozone as well as  
75 other secondary pollutants to a specified emission reduction (50%) for winter and summer  
conditions (January and July 2018). Our results indicate that, in winter, a 50% decrease in  
nitrogen oxide (NO<sub>x</sub>) emissions leads to an increase in surface O<sub>3</sub> concentrations of 15%–33%  
on average across China. In summer, the concentration of O<sub>3</sub> increases by up to 17% in the  
areas limited by the level volatile organic compounds (VOCs), while it decreases by 3%–12%  
80 in NO<sub>x</sub>-limited areas. The increase in the ozone concentration is associated with a reduced  
NO<sub>x</sub>-titration effect and higher levels of hydroxyl (OH) due to a reduced loss from reactions

85 with nitrogen dioxide (NO<sub>2</sub>). With a 50% reduction in anthropogenic VOCs (AVOCs)  
emissions, the O<sub>3</sub> concentration decreases across the entire geographic area, with reductions of  
4%–10% in South China during winter and 8%–20% in urban areas during summer. When  
combining the reductions in NO<sub>x</sub> and AVOCs emissions, the ozone response in urban areas  
(VOC-limited) is determined by the positive effect of NO<sub>x</sub> emission reduction in winter and  
the negative effect of AVOCs emission reduction in summer. An exception is found in the  
response during summertime in South China, where the role of biogenic VOCs in ozone  
formation is crucial due to relatively high temperatures and the existence of vegetation  
90 surroundings.

95 Summertime increases in the concentration of oxidized VOCs (OVOCs), particularly  
aldehydes and alcohols, are attributable to the reduction in NO<sub>x</sub> emissions. This enhancement  
subsequently enhances the atmospheric oxidative capacity through the photolysis of OVOCs  
and the oxidation of alkenes by OH radicals; it favors the formation of ozone. A significant  
decrease in particulate nitrate and in secondary organic aerosols is derived following the  
reduction in NO<sub>x</sub> and AVOCs emissions, respectively. These reductions in the aerosol  
concentration contribute to O<sub>3</sub> formation, through enhanced levels of hydroperoxyl (HO<sub>2</sub>)  
radicals associated with a reduced loss via aerosol uptake, and a diminished aerosol extinction.  
100 To effectively mitigate ozone pollution in urban areas, simultaneous reductions in the emission  
of NO<sub>x</sub> and specific VOCs species should be applied, especially regarding alkenes, aromatics,  
and unsaturated OVOCs, including methanol and ethanol.

105 Keywords: ozone pollution, emission reduction, WRF-Chem~~nitrogen chemistry~~, AOC

110

115

## 1. Introduction

To effectively reduce air pollution in China, the government of the country has implemented stringent actions between 2013 and 2020 (Liu et al., 2020; Liu et al., 2023). In the initial phase, from 2013 to 2017, the control of primary pollutants was particularly effective, with a dramatic decrease in the anthropogenic emissions of fine particles (PM<sub>2.5</sub>), sulfur dioxide (SO<sub>2</sub>), and nitrogen oxides (NO<sub>x</sub>) (Zheng et al., 2018; Liu et al., 2020). In subsequent years, a sustained reduction in the emission of SO<sub>2</sub>, NO<sub>x</sub>, and PM<sub>2.5</sub> was achieved, particularly between 2018 and 2020 (Liu et al., 2023). The implementation of the emission control policies has greatly improved China's air quality. However, a significant increase in the surface ozone (O<sub>3</sub>) concentration was observed from 2013 to 2019, with the positive trend slowing down in 2020 and 2021, but rebounding in 2022 (Liu et al., 2023; China Air 2023). Several studies provide explanations for the positive trend observed in the surface O<sub>3</sub> concentration, including a reduction in NO<sub>x</sub> emissions and in the atmospheric aerosol loading (Li et al., 2019; Liu et al., 2020). During and after the recent COVID-19 lockdown period, ozone pollution has been reported to happen, which is believed to be favored by the sharp reduction of NO<sub>x</sub> and high emissions of volatile organic compounds (VOCs) (Li et al., 2021). Looking through these changes over the past decade, we learn that rapid reductions of emissions disturb the current ozone chemistry and, thereby, produce changes in the ozone concentrations.

The response of ozone to reduced NO<sub>x</sub> emissions varies with the local photochemical environment and specifically with the chemical regimes (i.e., VOC-limited, NO<sub>x</sub>-limited, or transition conditions) (Jacob., et al., 1995; Ou et al., 2016; Dai et al., 2023). In NO<sub>x</sub>-sensitive regimes, the reduction in NO<sub>x</sub> emissions decreases the amount of NO<sub>2</sub> molecules photolyzed, leading to fewer ozone molecules being produced. While, in VOC-sensitive regimes, the reduction in the NO<sub>x</sub> abundance tends to enhance the ozone formation due to the weakening of NO titration and the reduced loss of OH radical reacted with NO<sub>2</sub>. Several studies based on satellite observations (Wang et al., 2021) and regional models (Zhu et al., 2023) have shown that the reduction in anthropogenic emissions has generated a change in the geographical distribution of the ozone formation regimes in China. These studies have reported a shift of ozone sensitivity regimes from VOC-sensitive to transition and/or NO<sub>x</sub>-sensitive in many metropolitan and suburban regions of East China. The shift towards NO<sub>x</sub>-limited conditions facilitates the implementation of an efficient ozone control through the reduction in NO<sub>x</sub> emissions only. In the remaining VOC-sensitive and transition areas, NO<sub>x</sub> emission reduction fails to effectively mitigate ozone pollution. In this situation, a coordinated reduction in anthropogenic VOCs (AVOCs) emissions should be implemented to effectively limit the ozone formation (Liu et al., 2023; Zhu et al., 2023). The source of NO<sub>x</sub> in VOC-sensitive areas is mainly from fossil fuel combustion, while the emissions of AVOCs result from a broad range of industrial, transportation and residential sources (B. Li et al., 2021; C. Li et al., 2022). To establish a cost-effective control over AVOCs emissions, the contribution of different VOCs categories to ozone formation should be accurately accessed for different areas of China.

Formatted: Font color: Auto

165 The effect of aerosols on the O<sub>3</sub> formation has been considered in several modeling studies (Li  
et al., 2019; Liu et al., 2020). However, the influences of aerosol on the O<sub>3</sub> production are  
complex due to the different effects to be taken into consideration. (Tan et al., 2022; Dai et al.,  
2023). Understanding the changes in aerosol effects on the O<sub>3</sub> formation when the primary  
emissions are further reduced remains a necessary condition for implementing efficient air  
quality control policies.

170 Recent observational studies combined with a source apportionment approach using  
observation-based models have highlighted the role of anthropogenic VOCs species, including  
the alkenes, aromatics, and oxidized volatile organic compounds (OVOCs), in mitigating  
summertime ozone formation in urban areas in China (C. Li et al., 2022; W. Wang et al., 2023)  
175 regions. The notable contributions of OVOCs to the oxidizing capacity of the atmosphere (*AOC*)  
as well as the formation of secondary organic aerosols (SOA) have been of concern in the  
regions of Yangzi River Delta (YRD) (J. Li et al., 2022) and Pearl River Delta (PRD) (W.  
Wang et al., 2022). The important role of biogenic VOCs (BVOCs) has also been highlighted  
180 in vegetated rural and urban regions in China, since the oxidation of BVOCs can significantly  
contribute to the formation of ozone and aerosols in the PRD region (J. Wang et al., 2023;  
Zhang et al., 2023). However, a comprehensive evaluation of the changes in the contribution  
of different VOCs categories to *AOC* and in ozone chemistry due to the emission changes in  
different regions of China is still needed. Considering the necessity of implementing  
coordinated actions among large areas to further alleviate air pollution in China, regional  
185 chemical transport models are appropriate tools to assess the quantitative response of the  
formation of secondary pollutants and of the oxidizing capacity of the atmosphere to emission  
changes.

190 In the companion paper (Part 1; Dai et al., 2023), we used a regional chemical-meteorological  
model to quantify the relative contribution of different photochemical processes to the  
formation and destruction of near-surface photochemical radicals and ozone in different  
chemical environments in China. In Part 2 of the study, with the evaluated model, we assess  
the response of the photo-oxidative species and related parameters to an imposed reduction of  
primary emissions. This paper is structured as follows. Section 2 introduces the setups of the  
195 model system and describes the simulations performed for specified reductions in the emissions  
of primary pollutants. In Section 3, we first analyze the response of near-surface concentration  
of ozone to the emission reduction. Further, we derive the drivers for the ozone changes,  
including the associated changes in ozone precursors and intermediate to primary emission  
reduction. We also discuss the changes in the ozone formation regime. Finally, we describe the  
200 sensitivity of the atmospheric oxidative capacity (*AOC*) to the reduction in emissions. A  
summary and implication for policy making of our study is provided in Sec. 4.

## 2. Method

### 2.1. Model setting

Formatted: Font color: Auto

Formatted: Font color: Auto

210 We use the WRF-Chem model version 4.1.2 (Skamarock et al., 2019), coupled with the gas-  
phase chemistry mechanism MOZART (Emmons et al., 2010) and the aerosol module  
215 MOSAIC (Zaveri et al., 2008), to simulate the meteorological fields as well as the transport,  
the chemical and physical transformations of trace gases and aerosols. The months of January  
and July of 2018 were selected as representative months to conduct the simulations and to  
investigate the changes in secondary pollution and in the AOC in response to emission  
reductions during winter and summer, respectively. Compared to the standard version of the  
chemical mechanism, several updates of heterogeneous uptake on the surface of the ambient  
220 aerosol were implemented (Dai et al., 2023). As for the SOA formation, the main pathways  
result from the gas-phase oxidation of VOCs by atmospheric oxidants (OH, O<sub>3</sub>, and NO<sub>3</sub>) and  
from the heterogeneous formation of glyoxal SOA over the ambient aerosol (Knote et al.,  
2014). The model domain covers the whole geographical area of China. Analyses of modeling  
results at four urban sites (Beijing, Shanghai, Guangzhou, and Chengdu) were also performed.  
More detailed information on the model configuration, the model validation, and the sites  
selected for our analysis can be found in Part 1 of our paper Dai et al., (2023).

225 We adopt the Multi-resolution Emission Inventory (MEIC v1.3; <http://www.meicmodel.org/>)  
to represent anthropogenic emissions in China and the CAMS-GLOB-ANT v4.2 inventory  
(<https://eccad.aeris-data.fr/>) provided by the Copernicus Atmosphere Monitoring Service  
(CAMS) to account for the anthropogenic emissions in the Asian areas outside China. To  
explore the sensitivity of secondary pollution and of AOC to emission reduction, several  
sensitivity experiments were designed based on our emissions inputs of NO<sub>x</sub>, anthropogenic  
230 VOCs (AVOCs). As shown in Table S1 of the Supplementary Information, NO<sub>x</sub> emissions  
include the emissions of NO<sub>2</sub> and NO, AVOCs emissions include those of alkanes [ethane  
(C<sub>2</sub>H<sub>6</sub>), propane (C<sub>3</sub>H<sub>8</sub>), and BIGALK (alkanes with carbon number ≥ 4)], alkenes [ethene  
(C<sub>2</sub>H<sub>4</sub>), propene (C<sub>3</sub>H<sub>6</sub>), and BIGENE (alkenes with carbon number ≥ 4)], aromatics [benzene  
(C<sub>6</sub>H<sub>6</sub>), toluene (C<sub>6</sub>H<sub>5</sub>CH<sub>3</sub>), and xylene (C<sub>6</sub>H<sub>4</sub>(CH<sub>3</sub>)<sub>2</sub>)], alkyne (C<sub>2</sub>H<sub>2</sub>), isoprene (C<sub>5</sub>H<sub>8</sub>),  
235 terpenes (C<sub>10</sub>H<sub>16</sub>), and OVOCs [methanol (CH<sub>3</sub>OH), ethanol (C<sub>2</sub>H<sub>5</sub>OH), acetaldehyde  
(CH<sub>3</sub>CHO), acetone (CH<sub>3</sub>COCH<sub>3</sub>), methacrolein (CH<sub>2</sub>CCH<sub>3</sub>CHO; MACR), and methyl vinyl  
ketone (CH<sub>2</sub>CHCOCH<sub>3</sub>; MVK)]. The emissions of ammonia (NH<sub>3</sub>), sulfur dioxide (SO<sub>2</sub>), and  
carbon monoxide (CO) are also considered.

## 240 2.2. Design of numerical experiment

245 To explore the sensitivity of secondary pollutants to emissions changes, five numerical  
experiments are conducted for January and July of 2018, respectively (Table 1). In the baseline  
case, denoted as “BASE”, we adopted the emissions described in Sect. 2.1. The concentrations  
of the key species calculated in this specific case have been validated in our companion study  
(Dai et al., 2023). To quantify the sensitivity of pollutants to potential mitigation policies, we  
apply uniform reductions in the surface emissions of primary pollutants over the entire  
geographical area of China; In the first two cases, arbitrary 50% reduction are applied  
separately in NO<sub>x</sub> and AVOCs emissions relative to the baseline case. These two cases are  
250 labeled “NO<sub>x</sub>” and “AVOCs”, respectively. A third case in which the 50% reduction is applied  
to both NO<sub>x</sub> and AVOCs emissions is referred to as “N+A”. The difference between the

Formatted: Font color: Auto

“perturbed” concentrations of pollutants and chemical parameters relative to the baseline case provides an estimate of the response in secondary pollution and chemistry to emission reduction.

255 Additionally, a simulation labeled “TOTAL” assumes that all anthropogenic emissions under consideration (NO<sub>x</sub>, AVOCs, CO, SO<sub>2</sub>, and NH<sub>3</sub>) are simultaneously reduced by 50%. This particular case is used to explore the impact on the ozone formation of a reduction in the emission of CO (an ozone precursor) and of SO<sub>2</sub> and NH<sub>3</sub> (as aerosol precursors). The spatial distribution of the emission fluxes changes for the different cases is shown in Fig. S1.

### 260 3. Model results

#### 3.2.2 Response of ozone concentrations to emission reduction

265 First, we describe the changes in the surface concentration of ozone in response to the reduction in surface emissions. To support the discussion on the ozone changes induced by the emission reduction, we adopted an indicator to distinguish different ozone sensitivity regimes, which is the calculated ratio between the production rate of hydrogen peroxide (H<sub>2</sub>O<sub>2</sub>) and of nitric acid (HNO<sub>3</sub>) [ $P(\text{H}_2\text{O}_2)/P(\text{HNO}_3)$ ]. An area is assumed to be VOC-limited or NO<sub>x</sub>-limited if the adopted indicator  $P(\text{H}_2\text{O}_2)/P(\text{HNO}_3)$  is smaller than 0.06 or if it is larger than 0.2, respectively (Tonnesen and Dennis, 2000; Yang et al., 2020; Zhao et al., 2019; Dai et al., 2023). The regions with ratios between these two limits represent transition situations.

270 Figure 1 displays the spatial distribution of the changes in the surface concentration of ozone during daytime (06:00-19:00 Local Standard Time) resulting from a 50% reduction in the NO<sub>x</sub>, AVOCs, and combined NO<sub>x</sub> and AVOCs emissions for January and July 2018.

275 Winter conditions. In January, the 50% reduction in the NO<sub>x</sub> emissions (NO<sub>x</sub> case) enhances the surface ozone concentrations, with the largest increase derived in the YRD and PRD regions by 15-33% (6-12 ppbv; Fig. 1a). During wintertime, a large part of China is under a VOC-sensitive regime (Fig. S2a). Therefore, the ozone titration decreased by the reduced NO concentrations due to NO<sub>x</sub> emission reduction, resulting in a decrease in ozone destruction (Fig. S3a) and hence favoring an increase in the ozone concentration. If AVOCs emissions are reduced by 50% (AVOCs case), the surface ozone is reduced by 4-10% (2.0 to 8.0 ppbv; Fig. 1b) in the southern part of China. This ozone decrease is associated with the reduced levels of radicals (see Sec. 3.2.1) and hence a reduction in the ozone production (Fig. S4a).

280 In the combined emission reduction case (N+A case), the ozone response in VOC-limited areas follows the positive changes found in the NO<sub>x</sub>-reduction case, with an ozone increase of 4-9% (3.0-7.5 ppbv; Fig. 1c) in North China and in some urban regions in South China. Simultaneously, a slight ozone decrease is derived along the southern coast of China (5-8% or 2.0-4.5 ppbv). In these areas, the ozone sensitivity is under the control of the NO<sub>x</sub>. The ozone decrease is dominated by the negative ozone response to the AVOCs emission reduction. With

Formatted: Font color: Auto, Not Highlight

Formatted: Font color: Auto

Formatted: Font color: Auto, Not Highlight

Formatted: Font color: Auto

Formatted: Font color: Auto

Formatted

Formatted: Subscript

Formatted

Formatted: Font color: Auto

Formatted

Formatted: Font color: Auto

Formatted

Formatted: Font color: Auto

Formatted

Formatted: Font color: Auto

Formatted

Formatted: Font color: Auto

Formatted

Formatted: Font color: Auto

295 further emission reduction of the other species (*TOTAL* case), an ozone increase (4-6% or 3-5 ppbv; Fig. 1d) relative to the combined case is calculated in the southern part of China.

300 Summer conditions. In July, under the reduction in the NO<sub>x</sub> emissions, an increase in the surface ozone concentration of up to 17% (10 ppbv; Fig. 1e) is calculated in the urbanized regions of NCP, YRD, and PRD. These areas are typically located in VOC-limited areas (Fig. S2b); thus, the ozone increase is explained by the reduced ozone titration due to NO<sub>x</sub> emission reduction. At the same time, in NO<sub>x</sub>-limited areas, the calculated surface ozone concentration is reduced by 3-10% (2 to 8 ppbv), as a result of reduced photochemical formation under lower NO<sub>x</sub> concentrations. With the reduction of AVOCs emissions, the surface ozone concentration decreases by 8-20% (8.0-12.0 ppbv; Fig. 1f) in whole areas of China.

305 In the combined emission reduction case, the surface ozone concentration decreases by up to 15% (12 ppbv; Fig. 1g) in NO<sub>x</sub>-sensitive areas. In VOC-sensitive areas, the surface ozone concentration also decreases, which differs from the ozone changes during wintertime. This is explained by the fact that the loss of ozone due to NO<sub>x</sub> titration is rapidly compensated by the photochemically formation of ozone, since the ozone production rate during summertime is accelerated by the high temperature and photolysis rate (T. Wang et al., 2022). When the emission reduction is applied to all species under consideration, the ozone changes (Fig. 1h) relative to the combined case are smaller than the changes in winter, due to a consistently smaller reduction in aerosol concentrations (see Sec. 3.2.3).

315 Table 2 and Figure S5 provide quantitative information on the response of ozone at different urban locations for January and July. In winter (in January), the separated emission reduction in NO<sub>x</sub> and AVOCs results in ozone increase (by ~ppbv or ~%) and decrease (by ~ppbv or ~%) in all cities. The ozone changes in the N+A and TOTAL cases follow the ozone response in NO<sub>x</sub> case, with ozone increase by ~ppbv (or ~%) and by ~ ppbv (or ~%), respectively. In summer (in July), the NO<sub>x</sub> emission reduction also results in ozone increases (by ~ ppbv or ~%) in all cities, while the AVOCs emission reduction results in decreases in all cities (by or). At the same time, in the N+A and TOTAL cases, ozone decreases can be found in Beijing (by ~ppbv or ~%), Shanghai (by ~ppbv or ~%), and Chengdu (by ~ppbv or ~%). One exception can be found at the Guangzhou site, where ozone increases by 0.5 ppbv (1~2%).

325 ~~This increase of ozone is consistent with the increase of OH radical and OVOCs at this site, which is related to the increasingly important role played by naturally emitted BVOCs species in the oxidation processes when anthropogenic emissions are reduced (see Sec. 3.3).~~

### 330 **3.12. Changes in precursors and intermediates in ozone formation**

335 In this section First, we describe the changes in the surface concentration of ozone precursors and intermediates, including the hydroxyl (OH) radical, the hydroperoxyl (HO<sub>2</sub>) radical, and specific oxidized volatile organic compounds (OVOCs) species in response to the reduction in surface emissions. To support the discussion on the radical changes induced by the emission reduction, we examine the changes in two specific parameters: the production rate of RO<sub>x</sub>

Formatted: Font: Italic, Font color: Auto

Formatted: Font color: Auto

Formatted: Font: (Asian) 新細明體, Font color: Auto, (Asian) Chinese (Traditional, Taiwan), Not Strikethrough

Formatted: Font color: Auto

Formatted: Font color: Auto, Subscript

Formatted: Font color: Auto

Formatted: Font color: Auto

Formatted: Font color: Auto, Subscript

Formatted: Font color: Auto

Formatted: Font color: Auto, Strikethrough, Not Highlight

Formatted: Font color: Auto, Strikethrough

Formatted: Font color: Auto

Formatted: Font: Bold, Font color: Auto

Formatted: Font color: Auto

Formatted: Font color: Auto, Not Highlight



radicals ( $P(\text{RO}_x)$ ) and the destruction rate of  $\text{RO}_x$  radicals ( $D(\text{RO}_x)$ ) (Tan et al., 2019). The production rate of  $\text{RO}_x$  radicals ( $P(\text{RO}_x)$ ) includes the photolysis of  $\text{O}_3$ , of nitrous acid (HONO), and of different OVOCs, and the ozonolysis of alkenes. The destruction rate of  $\text{RO}_x$  radicals ( $D(\text{RO}_x)$ ) results from the termination reactions between different  $\text{RO}_x$  radicals and between  $\text{RO}_x$  radicals with nitric oxide as well as from the heterogeneous uptake of  $\text{HO}_2$  on aerosol surfaces. Detailed model estimates of  $P(\text{RO}_x)$  and  $D(\text{RO}_x)$  can be found in Part 1 of the present study (Dai et al., 2023).

### 3.4.2.1. Changes in radicals

*Winter conditions.* Figure 4-2 displays the spatial distribution of the changes in the surface daytime (06:00-19:00 ~~Local Standard Time~~) mixing ratios of OH and  $\text{HO}_2$  radicals resulting from a 50% reduction in the  $\text{NO}_x$ , AVOCs, and combined  $\text{NO}_x$  and AVOCs emissions for January 2018. With the reduction in  $\text{NO}_x$  emissions (*NO<sub>x</sub> case*), the calculated mixing ratio of the surface OH radical is decreased in southern China by up to 40% (0.05 pptv; Fig. 4a2a), with a lower reduction in the central and western parts of the country. The decreases in the  $\text{NO}_2$  concentration (Fig. S2aS6a), resulting from the reduced  $\text{NO}_x$  emissions, lead to the reduced formation of ozone. As a result, the oxidation capacity and levels of oxidants are smaller than in the *BASE* case (see Sect. 3.3). At the same time, an increase in the concentration of the OH radical is found in urban areas, including the North China Plain (NCP), Yangzi River Delta (YRD), Pearl River Delta (PRD), and Si Chuan Basin (SCB) regions, with a maximum increase of 24% in the PRD region. This increase results from the reduced loss of the OH radical by the reaction with  $\text{NO}_2$  (Fig. S2bS6b). A distinct increase in the surface mixing ratio of  $\text{HO}_2$  radical is derived in southern China (by up to 5 pptv or 60%; Fig. 4b2c), which contributes to an increase of ozone with the reaction with NO. The enhancement of  $\text{HO}_2$  is related to the increased mixing ratio of the OH radical found in urban areas, resulting in enhanced  $\text{HO}_2$  levels via VOCs oxidation, and a reduced  $\text{HO}_2$  loss via the aerosol uptake, as the aerosol load is reduced (see Sect. 3.2.3.1) (Song et al., 2021).

For the 50% decrease in AVOCs emissions (*AVOCs case*), the mixing ratio of OH is reduced by 4-12% (0.005-0.015 pptv; Fig. 4e2b) and the mixing ratio of  $\text{HO}_2$  radicals by 20-36% (1-3 pptv; Fig. 4d2f) in the southern part of China. The decrease in the mixing ratio of these radicals is related to the reduced oxidation rate of VOCs, due to the decrease in the concentration of hydrocarbons (Fig. S3aS7a), whose emissions are reduced. The production of  $\text{RO}_x$  also decreases due to the reduced AVOCs emissions, especially from the photolysis of formaldehyde (HCHO), and other OVOCs (Fig. S3bS7b,-c). Simultaneously, a slight increase in the mixing ratio of OH radical is derived in the southern part of China. This increase in the OH radical is related to the reduced extinction of radiation associated with the decreased aerosol load due to the AVOCs emission reduction.

When the 50% emission reduction in  $\text{NO}_x$  is combined with the 50% reduction in AVOCs emissions (*N+A case*), the distribution of changes in the OH radical are similar to the pattern induced by emission reduction in  $\text{NO}_x$  alone. However, a weakened increase is calculated, as the increase in OH radical with reduced  $\text{NO}_x$  emissions is largely compensated by the decreased

radical concentrations following the AVOCs emission reduction. As shown in Fig. 4e2c, the maximum increase in urban China is lowered to 12% (from 40%). The increase in the mixing ratio of HO<sub>2</sub> radicals is reduced to 20% (from 60%; Fig. 4f2g), with only a mild increase distributed along the southern coast of China.

When accounting for the additional reduction in other anthropogenic emissions (NH<sub>3</sub>, SO<sub>2</sub>, and CO) (*TOTAL* case), the mixing ratio of the OH radical is positively modified, relative to the results in the combined case (*N+A* case). As shown in Fig. 2S4da, the mixing ratio of the OH radical is enhanced in the PRD and SCB regions (by up to 22%). This increase is due to the lowered consumption of the OH radical by the reduced concentration of carbon monoxide (CO) (Fig. S5aS8a), due to its reduced emissions (Fig. S1d). For the HO<sub>2</sub> radicals, the additional reduction in the other emissions also contributes to a larger mixing ratio, with a pronounced increase in southern China (by up to 18%; Fig. 2S4eh). This increase in the HO<sub>2</sub> radical mixing ratio is due to the increase in the oxidation of the VOCs by the OH radical and the reduced aerosol uptake of HO<sub>2</sub> associated with the decrease in the aerosol load.

*Summer conditions.* Figure 2-3 displays the spatial distribution of the changes in the surface daytime mixing ratio of the OH and HO<sub>2</sub> radicals due to the applied reduction in NO<sub>x</sub>, AVOCs, and combined NO<sub>x</sub> and AVOCs emissions for July 2018. Compared with the wintertime variation in radicals, which is limited to southern China, the geographical area covered by these summertime changes covers a larger fraction of China, including the northern provinces. When applying a 50% reduction in the NO<sub>x</sub> emissions, the mixing ratio of the OH radicals decrease in large parts of China, with the maximum decrease reaching 40% (0.15 pptv; Fig. 2a3a). The concentration of the OH radical increases in the metropolitan areas, including in the YRD and PRD regions. Simultaneously, the surface mixing ratio of the HO<sub>2</sub> radical increases by 15-20% (6 to 8 pptv; Fig. 2d3e) in the North China Plain. The differences in the distribution of radicals between winter and summer is due to the season patterns of meteorological parameters including temperature, water vapor abundance, and solar radiation intensity, which affect the oxidative processes (Dai et al., 2023) These changes are affected by meteorological parameters including the temperature, the water vapor abundance, and the solar radiation intensity, which affect the oxidative processes (Dai et al., 2023).

When AVOCs emissions are reduced by 50%, the mixing ratio of the radicals in urban areas, including in the NCP, YRD, and PRD regions, decreases on average by 8-12% in the case of OH (0.03-0.05 pptv; Fig. 2b3b) and by 6-10% in the case of HO<sub>2</sub> (3-5 pptv; Fig. 2e3f). When applying the combined 50% emission reduction in AVOCs and NO<sub>x</sub>, the changes in the patterns of the OH radical are similar to the distribution derived for the reduction in NO<sub>x</sub> emissions alone, but it is also partially offset by the counteracting effect of AVOCs emissions, as for winter conditions. As shown in Fig. 2e3c, the maximum increase in OH radical is reduced to 20% (from 40%) and the maximum decrease to 12% (from 30%). The counteracting effect of AVOCs emission reduction is also shown in the enhanced abundance of HO<sub>2</sub> radicals (Fig. 2f3g), with less than 6% (from 15-20%) increases in the urban areas.

Formatted: Font color: Auto

425 With an additional 50% reduction in other anthropogenic emissions, the changes in OH and  
HO<sub>2</sub> radicals relative to the results in the combined case are smaller than the changes in winter  
conditions (Fig. S4b-3d and eh). This is due to the relevant small decrease in aerosol load  
during summer (see Sec. 3.2.3). ~~A spatial shift in the ozone decrease area, from the southern  
430 regions in winter to the northern regions in summer occurs under this condition; this change is  
consistent with the spatial distribution of the reduction in the mixing ratio of the HO<sub>2</sub> radical,  
which contributes to the ozone production by its reaction with nitric oxide (Fig. S15b).~~

Formatted: Font color: Auto, Not Highlight

Formatted: Font color: Auto

Formatted: Font color: Auto, Strikethrough

Formatted: Font color: Auto

### 435 3.4.2.2 Changes in OVOCs

Oxygenated hydrocarbons (OVOCs) originate from direct biogenic and anthropogenic surface  
emissions (primary source), and from the oxidation of primary hydrocarbons (secondary  
source) in the atmosphere (W. Wang et al., 2022).

440 *Winter conditions.* Figure 3-4 shows the spatial distribution of the calculated changes in total  
OVOCs due to a 50% reduction in NO<sub>x</sub>, AVOCs and in combined NO<sub>x</sub> and AVOCs emissions  
for January of 2018. With the adopted reduction in NO<sub>x</sub> emission, the OVOCs concentration  
decreases in the non-urban areas of southern China and increases in urbanized China (Fig.  
445 3a4a), which is consistent with the changes derived for the mixing ratio of the OH radical. The  
highest increase in the OVOCs concentration is approximately 10% (2 ppbv) in the urban areas  
of the YRD and PRD regions; it includes a significant increase in the concentration of  
formaldehyde (HCHO; Fig. S6aS9a), followed by peroxyacetyl nitrate (PAN; Fig. S6bS9b),  
and alcohols (CH<sub>3</sub>OH and C<sub>2</sub>H<sub>5</sub>OH; Fig. S6eS9c). At the four city sites under consideration,  
450 the highest increase in OVOCs is calculated at Shanghai and Guangzhou, with concentrations  
increasing by about 12% (1.8 ppbv; Fig. 3e4f) and 8% (1.2 ppbv; Fig. 3f4g), respectively.

When the AVOCs emissions are reduced, the abundance of OVOCs is reduced in ~~most-all~~  
regions of China (Fig. 3b4b), with the highest decrease found in the regions of PRD and SCB.  
At the four city sites under consideration (Fig. 3d4e-gh), the decrease is the most pronounced  
455 in the concentration of ketones, including acetone (CH<sub>3</sub>COCH<sub>3</sub>), methyl vinyl ketone  
(CH<sub>3</sub>C(O)CHCH<sub>2</sub>), and methyl ethyl ketone (CH<sub>3</sub>CH<sub>2</sub>C(O)CH<sub>2</sub>CH<sub>3</sub>). The abundance of these  
species is reduced by almost a factor of two, followed by HCHO and other aldehydes. When  
combining the emission reduction of AVOCs and NO<sub>x</sub>, the decrease in OVOCs concentration  
resulting from the AVOCs emission reduction is further strengthened in large parts of China  
460 (Fig. 3e4c). However, an increased mixing ratio of 1~2 ppbv is derived for OVOCs at the  
Guangzhou site (Fig. 3f4f), which is consistent with an increase in the mixing ratio of OH  
radical at this site (Fig. S7S10). With additional decreases in the other emissions, the OVOCs'  
concentration is enhanced by 2~4 ppbv in whole China (Fig. S4e4d), which is consistent with  
465 the increased abundance of the OH radical resulting from a reduction in the NH<sub>3</sub>, SO<sub>2</sub>, and CO  
emissions.

*Summer conditions.* Figure 4-5 displays the spatial distribution of the changes in total OVOC  
concentrations in response to a 50% reduction in NO<sub>x</sub>, AVOCs and in the combined NO<sub>x</sub> and

470 AVOCs emissions for July 2018. With a 50% reduction in NO<sub>x</sub> emissions, the changes in the  
475 OVOCs concentrations do not resemble the changes in the concentrations of the OH radical. A  
480 decrease in the OVOCs is derived in southern China. However, in central and northern China,  
the level of OVOCs generally increases and this increase is not limited to metropolitan areas  
(Fig. 4a5a). For specific OVOCs, the changes in HCHO, glyoxal, and PAN (Fig. S8aS11a-c)  
are consistent with the changes calculated for the OH radical. However, for aldehydes and  
alcohols (Fig. S9aS12a,-b), an increased concentration is derived in the entire geographical  
area of China, with a consistent distribution of changes in alkenes (Fig. S9eS12c) and isoprene  
(Fig. S9dS12d). In summer, the temperature-dependent emissions of biogenic VOCs from  
vegetation are high (Zhang et al., 2023). The reduced production rate of OVOCs, resulting  
from the reduced AVOCs emissions, is compensated to a certain degree by the high natural  
emissions of BVOCs species.

485 With a 50% reduction in AVOCs emission, the OVOCs concentrations are significantly  
490 reduced in the NCP and SCB regions (Fig. 4b5b). Different from what is occurring in winter  
(OVOCs concentration reduced by about 50%), the response of the OVOCs to the AVOCs  
emission reduction is milder in summer, with the largest decrease being reduced to 30%. This  
is explained by the more effective secondary formation of OVOCs during summertime.  
Nevertheless, a more pronounced decrease in OVOC abundance is found in North China. For  
example, at the Beijing site, the decreases in OVOCs concentration reaches 10 ppbv compared  
to the 5 ppbv derived in winter, which is consistent with the higher concentration of  
summertime OVOCs (~34 ppbv) relative to winter (~11 ppbv). When the combined reduction  
in the emissions of AVOCs with NO<sub>x</sub> are considered, a lower decrease of OVOCs is found in  
the geographical area of China (Fig. 4e5c), which is relevant to the reduced decrease in the OH  
concentration. The response on the OVOCs concentration to the reduced emissions applied to  
the other species under consideration is small (Fig. 4Sf5d).

### 495 3.2. Changes in secondary pollutants to emission reduction

500 ~~The formation of ozone and secondary aerosol is affected by the changes in the emissions of  
primary organic species and in the concentration of ozone precursors and intermediate species.  
In order to highlight the regional differences in the response of the existing photochemical  
regimes to emission reduction, we first show the changes in the distributions of the areas where  
the ozone formation is either NO<sub>x</sub>- or VOC-limited. We distinguish the two regions from the  
calculated ratio between the production rate of hydrogen peroxide (H<sub>2</sub>O<sub>2</sub>) and of nitric acid  
(HNO<sub>3</sub>) [ $P(\text{H}_2\text{O}_2)/P(\text{HNO}_3)$ ]. An area is assumed to be VOC-limited or NO<sub>x</sub>-limited if the  
adopted indicator  $P(\text{H}_2\text{O}_2)/P(\text{HNO}_3)$  is smaller than 0.06 or if it is larger than 0.2, respectively  
(Tonnesen and Dennis, 2000; Yang et al., 2020; Zhao et al., 2019). The regions with ratios  
between these two limits represent transition situations. The production rate of odd oxygen ( $\text{O}_x$   
 $\equiv \text{O}_3 + \text{NO}_2$ ), associated with recurrent radical reaction chains involving the oxidation of  
hydrocarbons in the presence of NO<sub>x</sub> ( $P(\text{O}_x)$ ), and the photochemical destruction rate of  $\text{O}_x$   
( $D(\text{O}_x)$ ), is also adopted here to support the analysis of the underlying reasons for the calculated  
ozone changes. The detailed definition of  $P(\text{O}_x)$  and  $D(\text{O}_x)$  can be found in Dai et al., (2023).~~

### 3.2.1 Response of ozone sensitivity regimes to emission reduction

Figure 5 displays the spatial distribution of ozone regimes in response to applied emission reductions for the emissions of  $\text{NO}_x$ , AVOCs and for combined  $\text{NO}_x$  and AVOCs emissions in January and July.

*Winter conditions.* In January, with a 50% reduction in  $\text{NO}_x$  emissions, the regions characterized by transition or VOC limited regimes in the south and southwest of China (in *BASE* case; Fig. 5a) tend to be converted into  $\text{NO}_x$  limited areas regarding ozone production (Fig. 5b). The change in the ozone sensitivity regimes is consistent with (1) the decreased concentration in the simulated  $\text{HNO}_3$  (Fig. S10a) due to less  $\text{NO}_2$  reacting with OH, and (2) the increased  $\text{H}_2\text{O}_2$  concentration (Fig. S10e) due to the reduced aerosol  $\text{HO}_2$  uptake by aerosols. With a 50% reduction in AVOCs emissions, some transition areas of southern China are converted to VOC limited areas (Fig. 5c). A relevant decrease in the  $\text{H}_2\text{O}_2$  concentration is also derived in southern China and is attributed to the decrease in the calculated  $\text{HO}_2$  concentration. When considering the combined reduction in  $\text{NO}_x$  and AVOCs emissions as well as the reduction in all anthropogenic emissions, the VOC limited regions of southern China evolve towards a transition region or even a  $\text{NO}_x$  limited region (Fig. 5d; Fig. S11a). In these two last cases, the changes in ozone sensitivity regimes are determined by the decrease in the calculated  $\text{HNO}_3$  concentrations (Fig. S10 c-d). At the urban sites, the emission reduction does not modify the wintertime ozone sensitivity regimes (Fig. S12), which remain VOC limited.

*Summer conditions.* In July, the changes in ozone regimes related to emission reductions are found mainly in VOC limited areas and in their surroundings, due to consistent changes in  $\text{H}_2\text{O}_2$  and  $\text{HNO}_3$  (Fig. S13). With the reduction of  $\text{NO}_x$  emissions, the size of VOC limited areas (Fig. 5e) shrinks and becomes a smaller fraction of the urbanized areas (Fig. 5f). At four urban sites (VOC limited in *BASE* case), the ozone sensitivity of Beijing sites is converted to  $\text{NO}_x$  limited (Fig. 5i). The sites of Shanghai (Fig. 5j) and Chengdu (Fig. 5l) are shifted to a Transition area. Only the Guangzhou site remains in a VOC limited region (Fig. 5k). With the reduction in AVOCs emissions, the VOC limited areas expand to the surroundings of the metropolitan areas (Fig. 5g). Finally, when considering the combined 50% reduction in the emissions of  $\text{NO}_x$  and AVOCs (*N+A* case; Fig. 5h) as well as the reduction of all other emitted species (*TOTAL* case; Fig. S11b), the pattern of calculated change in the ozone sensitivity is similar to the pattern corresponding to the  $\text{NO}_x$  emissions, with a smaller VOC limited area relative to the *BASE* case. In these cases, the sites of Beijing and Chengdu shift to a transition condition, while the Guangzhou and Shanghai sites remain under VOC limited conditions.

### 3.2.2 Response of ozone concentrations to emission reduction

Figure 6 shows the changes in daytime (06:00 to 19:00 LST) surface ozone concentrations resulting from a 50% reduction of the  $\text{NO}_x$  and AVOCs emissions in January and July of 2018.

*Winter conditions.* In January, the 50% reduction in the  $\text{NO}_x$  emissions enhances the surface ozone concentrations, with the largest increase derived in the YRD and PRD regions by 15-

33% (6–12 ppbv; Fig. 6a). During wintertime, a large part of China is under a VOC sensitive regime. Therefore, the reduced titration of ozone by reduced NO<sub>x</sub> concentrations (Fig. S14a; Fig. S2e) favors an increase in the ozone concentration. If AVOCs emissions are reduced by 50%, the surface ozone is reduced by 4–10% (2.0 to 8.0 ppbv; Fig. 6b) in the southern part of China. This ozone decrease is associated with the reduced concentration of HO<sub>x</sub> radicals and hence a reduction in the ozone production by the HO<sub>2</sub>+NO reaction (Fig. S15a).

In the combined emission reduction case, the ozone response in VOC limited areas follows the positive changes found in the NO<sub>x</sub> reduction case, with an ozone increase of 4–9% (3.0–7.5 ppbv; Fig. 6c) in North China and in some urban regions in South China. Simultaneously, a slight ozone decrease is derived along the southern coast of China (5–8% or 2.0–4.5 ppbv). In these areas, the ozone sensitivity is under the control of the NO<sub>x</sub>. The ozone decrease is dominated by the negative ozone response to the AVOCs emission reduction. With further emission reduction of the other species, an ozone increase (4–6% or 3–5 ppbv; Fig. S4g) relative to the combined case is calculated in the southern part of China, resulting from the increased HO<sub>2</sub> radical (Fig. S4c) reacted with NO.

*Summer conditions.* In July, under the reduction in the NO<sub>x</sub> emissions, an increase in the surface ozone concentration of up to 17% (10 ppbv; Fig. 6d) is calculated in the urbanized regions of NCP, YRD, and PRD. These areas are typically located in VOC limited areas; thus, the ozone increase is explained by the reduced ozone titration (Fig. S14b). At the same time, in NO<sub>x</sub> limited areas, the calculated surface ozone concentration is reduced by 3–10% (2 to 8 ppbv), as a result of reduced photochemical formation under lower NO<sub>x</sub> concentrations. With the reduction of AVOCs emissions, the surface ozone concentration decreases by 8–20% (8.0–12.0 ppbv; Fig. 6e) in whole areas of China. A spatial shift in the ozone decrease area, from the southern regions in winter to the northern regions in summer occurs under this condition; this change is consistent with the spatial distribution of the reduction in the mixing ratio of the HO<sub>2</sub> radical, which contributes to the ozone production by its reaction with nitric oxide (Fig. S15b).

In the combined emission reduction case, the surface ozone concentration decreases by up to 15% (12 ppbv; Fig. 6f) in NO<sub>x</sub> sensitive areas. In VOC sensitive areas, the surface ozone concentration also decreases, which differs from the ozone changes during wintertime. This is explained by the fact that the loss of ozone due to NO<sub>x</sub> titration is rapidly compensated by the photochemically formation of ozone, since the ozone production rate during summertime is accelerated by the high temperature and photolysis rate (T. Wang et al., 2022). One exception can be found at the Guangzhou site, where ozone increases by 0.5 ppbv (1–2%; Fig. S16). This increase of ozone is consistent with the increase of OH radical and OVOCs at this site, which is related to the increasingly important role played by naturally emitted BVOCs species in the oxidation processes when anthropogenic emissions are reduced (see Sec. 3.3). When the emission reduction is applied to all species under consideration, the ozone changes (Fig. S4h) relative to the combined case are smaller than the changes in winter, due to a consistently smaller reduction in aerosol concentrations (see Sec. 3.2.3).

### 3.2.3. Changes in aerosol

Figure 6 shows the changes in the average concentrations of secondary aerosol due to emission reduction in January and July of 2018.

*Winter conditions.* In January, the 50% reduction of  $\text{NO}_x$  leads to a large decrease in the aerosol load ( $10\text{-}18 \mu\text{g m}^{-3}$  or  $12\text{-}20\%$ ; Fig. 6a) of central and southern China. The aerosol decrease predominantly results from the decrease in the  $\text{NO}_3^-$  abundance (Fig. S13a) linked to the reduced concentration of  $\text{NO}_2$ , followed by reduction in the concentration of  $\text{NO}_4^+$  (Fig. S13b). A slight increase in the abundance of secondary organic aerosols (SOA) is derived in the urban areas of NCP, YRD, and PRD regions ( $1\text{-}2 \mu\text{g m}^{-3}$  or  $3\text{-}5\%$ ; Fig. S13c), which is consistent with the increase in the level of oxidants, including ozone and OH radicals. With a 50% reduction of AVOCs emissions, the changes in the aerosol concentration are smaller than with the 50% reduction in  $\text{NO}_x$  emissions, with a decrease of less than 4% ( $5 \mu\text{g m}^{-3}$ ; Fig. 6b), which predominantly results from the reduction in SOA (Fig. S14a). With a joint reduction in  $\text{NO}_x$  and AVOCs (Fig. 6c), the aerosol decrease is larger than the separated effect of the individual emissions decrease, as the increase in the concentration of SOA resulting from the reduced  $\text{NO}_x$  emissions is compensated by the reduced AVOCs emissions.

With a further reduction in other emissions, the decrease in the concentration of aerosol is deeply enhanced; this is the case for the concentration of  $\text{NH}_4^+$  (Fig. S15a),  $\text{SO}_4^{2-}$  (Fig. S15b), and  $\text{NO}_3^-$  particles (Fig. S15c). The concentration of the gas-phase precursors,  $\text{NH}_3$  and  $\text{SO}_2$ , is considerably reduced, which affects the process of acid replacement (Meng et al., 2022) and hence the level of  $\text{NO}_3^-$ . In our model, the concentration of  $\text{NO}_2$  and  $\text{PM}_{2.5}$  is overestimated for the baseline conditions (Dai et al., 2023), which can possibly lead to an excessively high reduction in aerosol concentration, especially in the concentration of  $\text{NO}_3^-$ . This overestimation potentially affects the aerosol-related changes in ozone formation.

*Summer conditions.* In July, the decrease in aerosol load due to the emission reduction is much smaller than in winter. The reduction ranges from  $1.5$  to  $5 \mu\text{g m}^{-3}$  (Fig. 6d), from  $2$  to  $6 \mu\text{g m}^{-3}$  (Fig. 6e), from  $4$  to  $7 \mu\text{g m}^{-3}$  (Fig. 6f) and from  $8$  to  $10 \mu\text{g m}^{-3}$  (Fig. 6g), for the reduction in the  $\text{NO}_x$ , AVOCs, combined  $\text{NO}_x$  and AVOCs, and *TOTAL* emissions, respectively. Similar with the ozone changes, the simulated reductions in aerosols also undergo a spatial shift, from the southern part of China in winter to the northern China Plain in summer. This shift is consistent with the calculated changes in oxidants, hydrocarbons, and other gaseous aerosol precursors. The higher decrease in the aerosols loads for the combined case also indicates that the reduction in AVOCs emission increases the efficiency of the aerosol decrease produced by the reduced  $\text{NO}_x$  emissions.

The aerosol effect on the ozone formation has been discussed in several modeling studies (Li et al., 2019; Liu et al., 2020; Dai et al., 2023). Our results show that the reduction in primary emissions results in a large decrease of aerosol concentrations. The major contribution to the aerosol decreases results from the reduction in  $\text{NO}_x$  emissions, with a strengthened effect when combined with a reduction in the AVOCs emissions. This decrease in the aerosol burden



645 weakens the aerosol extinction effect and therefore enhances the photochemical formation rate  
of radicals and ozone. As shown in Fig. S16a-d, the photolysis rate increases (by 5-20%) in  
southern and central China during winter due to the aerosol decrease induced by the emission  
reductions. The highest increase in photolysis rates results from the joint emission reduction in  
650 NO<sub>x</sub> and AVOCs (Fig. S16c). The increase of the photolysis rates in summer is not as distinct  
as the increase during wintertime due to the more limited reduction of the aerosol burden during  
summer (Fig. S16e-h).

Formatted: Font color: Auto

655 Further, the reduction in the aerosol burden lowers the aerosol uptake of NO<sub>2</sub> and HO<sub>2</sub> radicals,  
which indirectly enhances the mixing ratio of OH and HO<sub>2</sub> radicals (Dai et al., 2023). An  
increased level of HO<sub>x</sub> (Fig. 2d, h; Fig. 3d, h) following the emission reduction in NH<sub>3</sub> and  
SO<sub>2</sub> can be caused by the reduced aerosol uptake, associated with a large decrease in the  
calculated concentrations of NH<sub>4</sub><sup>+</sup> and SO<sub>4</sub><sup>2-</sup>. Large uncertainties still exit in the value of uptake  
coefficient of HO<sub>2</sub> used in the model (Yang et al., 2023), which affects the evaluation of aerosol  
660 effects on ozone concentration and deserved further studies in the future. In short, the reduction  
in the aerosol load is supportive of the ozone formation. Therefore, there is a need to consider  
the aerosol effect on ozone formation even with stringent emission reduction.

Formatted: Font color: Auto

### **3.3. Response of ozone sensitivity regimes to emission reduction**

Formatted: Font: Bold, Font color: Auto

665 The formation of ozone and secondary aerosol is affected by the changes in the emissions of  
primary organic species and in the concentration of ozone precursors and intermediate species.

Formatted: Font color: Auto

Formatted: Font: Bold, Font color: Auto

Formatted: Font color: Auto

Formatted: Font: Bold, Font color: Auto

Formatted: Font color: Auto

670 In order to highlight the regional differences in the response of the existing photochemical  
regimes to emission reduction, we first show the changes in the distributions of the areas where  
the ozone formation is either NO<sub>x</sub>- or VOC-limited.

Figure 7 displays the spatial distribution of ozone regimes in response to applied emission  
reductions for the emissions of NO<sub>x</sub>, AVOCs, for combined NO<sub>x</sub> and AVOCs emissions (N+A),  
and with additional other species (*TOTAL*) in January and July.

Formatted: Font: Italic, Font color: Auto

Formatted: Font color: Auto

675 *Winter conditions.* In January, with a 50% reduction in NO<sub>x</sub> emissions, the regions  
characterized by transition or VOC-limited regimes in the south and southwest of China (in  
BASE case; Fig. S2a) tend to be converted into NO<sub>x</sub>-limited areas regarding ozone production  
(Fig. 7a). The change in the ozone sensitivity regimes is consistent with (1) the decreased  
680 concentration in the simulated HNO<sub>3</sub> (Fig. S10a) due to less NO<sub>2</sub> reacting with OH, and (2) the  
increased H<sub>2</sub>O<sub>2</sub> concentration (Fig. S10e) due to the reduced aerosol HO<sub>2</sub> uptake by aerosols.  
With a 50% reduction in AVOCs emissions, some transition areas of southern China are  
converted to VOC-limited areas (Fig. 7b). A relevant decrease in the H<sub>2</sub>O<sub>2</sub> concentration is  
also derived in southern China and is attributed to the decrease in the calculated HO<sub>2</sub>  
685 concentration. When considering the combined reduction in NO<sub>x</sub> and AVOCs emissions as  
well as the reduction in all anthropogenic emissions, the VOC-limited regions of southern  
China evolve towards a transition region or even a NO<sub>x</sub>-limited region (Fig. 7c; Fig. 7d). In  
these two last cases, the changes in ozone sensitivity regimes are determined by the decrease



690 in the calculated HNO<sub>3</sub> concentrations (Fig. S17c, d). At the urban sites, the emission reduction  
695 does not modify the wintertime ozone sensitivity regimes (Fig. S18), which remain VOC-  
limited.

Summer conditions. In July, the changes in ozone regimes related to emission reductions are  
695 found mainly in VOC-limited areas and in their surroundings, due to consistent changes in  
H<sub>2</sub>O<sub>2</sub> and HNO<sub>3</sub> (Fig. S19). With the reduction of NO<sub>x</sub> emissions, the size of VOC-limited  
areas shrinks and becomes a smaller fraction of the urbanized areas (Fig. 7e). At four urban  
sites (VOC-limited in BASE case), the ozone sensitivity of Beijing sites is converted to NO<sub>x</sub>-  
limited (Fig. 7i). The sites of Shanghai (Fig. 7j) and Chengdu (Fig. 7l) are shifted to a Transition  
700 area. Only the Guangzhou site remains in a VOC-limited region (Fig. 7k). With the reduction  
in AVOCs emissions, the VOC-limited areas expand to the surroundings of the metropolitan  
areas (Fig. 7g). Finally, when considering the combined 50% reduction in the emissions of  
NO<sub>x</sub> and AVOCs (N+A case; Fig. 7g) as well as the reduction of all other emitted species  
(TOTAL case; Fig. 7h), the pattern of calculated change in the ozone sensitivity is similar to  
the pattern corresponding to the NO<sub>x</sub> emissions, with a smaller VOC-limited area relative to  
705 the BASE case. In these cases, the sites of Beijing and Chengdu shift to a transition condition,  
while the Guangzhou and Shanghai sites remain under VOC-limited conditions.

### 3.2.3. Response of aerosols to emission reduction

710 Figure 7 shows the changes in the average concentrations of secondary aerosol due to emission  
reduction in January and July of 2018.

Winter conditions. In January, the 50% reduction of NO<sub>x</sub> leads to a large decrease in the aerosol  
715 load (10–18 μg m<sup>-3</sup> or 12–20%; Fig. 7a) of central and southern China. The aerosol decrease  
predominantly results from the decrease in the NO<sub>3</sub><sup>-</sup> abundance (Fig. S17a) linked to the  
reduced concentration of NO<sub>2</sub>, followed by effect of NO<sub>4</sub><sup>+</sup> (Fig. S17b). A slight increase in the  
abundance of secondary organic aerosols (SOA) is derived in the urban areas of NCP, YRD,  
and PRD regions (1–2 μg m<sup>-3</sup> or 3–5%; Fig. S17e), which is consistent with the increase in the  
level of oxidants, including ozone and OH radicals. With a 50% reduction of AVOCs  
emissions, the changes in the aerosol concentration are smaller than with the 50% reduction in  
720 NO<sub>x</sub> emissions, with a decrease of less than 4% (5 μg m<sup>-3</sup>; Fig. 7b), which predominantly results  
from the reduction in SOA (Fig. S18a). With a joint reduction in NO<sub>x</sub> and AVOCs (Fig. 7c),  
the aerosol decrease is larger than the separated effect of the individual emissions decrease, as  
the increase in the concentration of SOA resulting from the reduced NO<sub>x</sub> emissions is  
compensated by the reduced AVOCs emissions.

725 With a further reduction in other emissions, the decrease in the concentration of aerosol is  
deeply enhanced; this is the case for the concentration of NH<sub>4</sub><sup>+</sup> (Fig. S19a), SO<sub>4</sub><sup>2-</sup> (Fig. S19b), and  
NO<sub>3</sub><sup>-</sup> particles (Fig. S19c). The concentration of the gas phase precursors, NH<sub>3</sub> and SO<sub>2</sub>, is  
considerably reduced, which affects the process of acid replacement (Meng et al., 2022) and  
730 hence the level of NO<sub>3</sub><sup>-</sup>. In our model, the concentration of NO<sub>2</sub> and PM<sub>2.5</sub> is overestimated  
for the baseline conditions, which can possibly lead to an excessively high reduction in aerosol

concentration, especially in the concentration of  $\text{NO}_3^-$ . This overestimation potentially affects the aerosol-related changes in ozone formation.

**Summer conditions.** In July, the decrease in aerosol load due to the emission reduction is much smaller than in winter. The reduction ranges from  $1.5$  to  $5 \mu\text{g m}^{-3}$  (Fig. 7d), from  $2$  to  $6 \mu\text{g m}^{-3}$  (Fig. 7e), from  $4$  to  $7 \mu\text{g m}^{-3}$  (Fig. 7f) and from  $8$  to  $10 \mu\text{g m}^{-3}$  (Fig. 7g), for the reduction in the  $\text{NO}_x$ , AVOCs, combined  $\text{NO}_x$  and AVOCs, and *TOTAL* emissions, respectively. Similar with the ozone changes, the simulated reductions in aerosols also undergo a spatial shift, from the southern part of China in winter to the northern China Plain in summer. This shift is consistent with the calculated changes in oxidants, hydrocarbons, and other gaseous aerosol precursors. The higher decrease in the aerosols loads for the combined case also indicates that the reduction in AVOCs emission increases the efficiency of the aerosol decrease produced by the reduced  $\text{NO}_x$  emissions.

The aerosol effect on the ozone formation has been discussed in several modeling studies (Li et al., 2019; Liu et al., 2020; Dai et al., 2023). Our results show that the reduction in primary emissions results in a large decrease of aerosol concentrations. The major contribution to the aerosol decreases results from the reduction in  $\text{NO}_x$  emissions, with a strengthened effect when combined with a reduction in the AVOCs emissions. This decrease in the aerosol burden weakens the aerosol extinction effect and therefore enhances the photochemical formation rate of radicals and ozone. As shown in Fig. S20 a-d, the photolysis rate increases (by 5-20%) in southern and central China during winter due to the aerosol decrease induced by the emission reductions. The highest increase in photolysis rates results from the joint emission reduction in  $\text{NO}_x$  and AVOCs (Fig. S20e). The increase of the photolysis rates in summer is not as distinct as the increase during wintertime due to the more limited reduction of the aerosol burden during summer (Fig. S20e-h).

Further, the reduction in the aerosol burden lowers the aerosol uptake of  $\text{NO}_2$  and  $\text{HO}_2$  radicals, which indirectly enhances the mixing ratio of OH and  $\text{HO}_2$  radicals (Dai et al., 2023). An increased level of  $\text{HO}_x$  (Fig. S4 a-d) following the emission reduction in  $\text{NH}_3$  and  $\text{SO}_2$  can be caused by the reduced aerosol uptake, associated with a large decrease in the calculated concentrations of  $\text{NH}_4^+$  and  $\text{SO}_4^{2-}$ . In short, the reduction in the aerosol load is supportive of the ozone formation. Therefore, there is a need to consider the aerosol effect on ozone formation even with stringent emission reduction.

### 3.34. Changes in atmospheric oxidative capacity

The Atmospheric Oxidizing Capacity (AOC) is a parameter that characterizes the self-cleansing ability of the atmosphere (Dai et al., 2023). It is derived here as the rate at which carbon monoxide (CO), methane ( $\text{CH}_4$ ), and non methane hydrocarbons (NMHCs) are oxidized by atmospheric oxidants, including OH,  $\text{O}_3$ , and  $\text{NO}_3$  (Xue et al., 2016; Dai et al., 2023). We derived the calculation of AOC as below.

Formatted: Font: Bold, Font color: Auto

Formatted: Font: Bold, Font color: Auto, Not Highlight

Formatted: Font: Bold, Font color: Auto

Formatted: Font color: Auto

Formatted: Font: Bold, Font color: Auto

Formatted: Font color: Auto

Formatted: Font: Bold, Font color: Auto

Formatted: Font color: Auto

Formatted: Font: Bold, Font color: Auto

Formatted: Font color: Auto

Formatted: Font: (Asian) SimSun

Formatted: Line spacing: Multiple 1.15 li, Border: Top: (No border), Bottom: (No border), Left: (No border), Right: (No border), Between : (No border)

775  $AOC = \sum_i^j k_{i,j} [Y_i] [X_j]$ .

780 Here the  $k_{i,j}$  represent the oxidized reaction rate between carbon monoxide (CO), methane (CH<sub>4</sub>), and non-methane hydrocarbons (NMHCs) (noted here as  $Y_i$ ) and the oxidants of OH radical, NO<sub>3</sub> radical as well as O<sub>3</sub> (noted as  $X_j$ ). It is derived here as the rate at which carbon monoxide (CO), methane (CH<sub>4</sub>), and non-methane hydrocarbons (NMHCs) are oxidized by atmospheric oxidants, including OH, O<sub>3</sub>, and NO<sub>3</sub> (Xue et al., 2016; Dai et al., 2023). This parameter allows us to characterize the formation process of O<sub>3</sub> and can be used as an indicator to design mitigation policies for reducing ozone pollution.

785 The changes in the spatial distribution of daytime (06:00 to 19:00 LST) AOC resulting from the adopted 50% reduction in the emissions of ozone precursors for January and July of 2018 are depicted in Fig. 8.

790 *Winter conditions.* In January, the 50% reduction in NO<sub>x</sub> emission leads to a decrease in daytime AOC of 10~20% in southern China and an increase of 10~18% in the urban areas, including the PRD, YRD and SCB regions (Fig. 8a). At the four city sites (Fig. 9 a-d), the increase in the daytime AOC is attributed to the enhanced contributions of the OH-related reactions, including the reactions of OH with alkenes, followed by the reaction of OH with OVOCs and with aromatics. This daytime AOC increase is consistent with the enhanced level in the OH radical, alkenes, and OVOCs when NO<sub>x</sub> emission reduced. During nighttime (20:00 to 05:00 LST), the reduction in NO<sub>x</sub> emissions is responsible for an increase in AOC by up to 50% (Fig. S21a-S20a). A contribution to this increase is provided by the alkenes' ozonolysis, since the concentration of ozone (Fig. 6a) and of alkenes is enhanced (Fig. S9e-S12c). The largest increase in the alkene ozonolysis is derived at the sites of Shanghai from 31% to 40% (Fig. S22b-S21b). These results highlight the promoted oxidative processes associated with the NO<sub>x</sub> emission reduction.

800 With the 50% reduction in AVOCs emissions, the daytime AOC is reduced in all the major regions of China (Fig. 8b), with the largest decreases occurring in the southern part of the country, with the largest decrease occurring at Guangzhou site (by 50%). This decrease in daytime AOC is mainly attributable to the reduced contribution from the reactions between OH and alkenes, followed by the reactions of OH with aromatics and with OVOCs. With a combined emission reduction in NO<sub>x</sub> and AVOCs emissions (Fig. 8c) and with the additional reduction in the other emissions considered here (Fig. S23a-S22a), the distribution patterns of the changes in daytime AOC are similar to the patterns found in the AVOCs cases but are characterized by higher decreases in daytime AOC.

815 *Summer conditions.* During summertime, the decrease in daytime AOC is more pronounced than in wintertime. With the 50% reduction in NO<sub>x</sub> emissions, daytime AOC decreases in large areas of China (ranging from 10% ~ 20%; Fig. 8d), while, in urban areas, an increase of is predicted, including the Guangzhou (8%; Fig. 9g), Shanghai (5%; Fig. 9f), and Chengdu (3%; Fig. 9h). However, at the Beijing site, the daytime value of AOC decreases (Fig. 9e), because

Formatted: Font: Italic

Formatted: Subscript

Formatted: Font color: Auto

Formatted: Font color: Auto, Not Highlight

Formatted: Font color: Auto

of the shift in the ozone sensitivity regime from VOC-limited to NO<sub>x</sub>-limited. During nighttime, the NO<sub>x</sub> emission reduction also leads to an increase in AOC due to the alkene ozonolysis (Fig. S21b-S20b), with the largest increase derived at the Beijing site (from 10% to 14%; Fig. S22e-S21e).

With other emission reduction cases (AVOCs, N+A, and TOTAL; Fig. 8e-f; Fig. S23b-S22b), the daytime AOC decreases in the entire China, with more distinct decreases in North China relative to winter conditions. With the reduction in the AVOCs emissions, the relative decrease of daytime AOC is smaller than in winter, especially at the Guangzhou site (to 30%), indicating a more important secondary formation of VOC-related AOC during summer. When the emissions of NO<sub>x</sub> and AVOCs are jointly reduced by 50%, the role of the reaction between OH and BVOCs in the determination of AOC is enhanced at the four city sites, with the largest increase (15%) found at the Guangzhou site. This increase results from the enhanced levels in OH radicals (Fig. 2c) and in biogenic VOCs species, such as isoprene (Fig. S24-S23).

The distribution patterns of changes in daytime AOC due to emission reduction is to a large extent consistent with the changes in the mixing ratio of the OH radicals and the changes in the concentration of OVOCs, ozone, and SOA in both winter and summer. These consistent patterns suggest that the AOC is an appropriate indicator to characterize the changes in secondary pollutants attributed to emission reduction. One exception is found when considering the changes in the ozone concentration resulting from the reduction in the NO<sub>x</sub> emission during winter. During this season, a comparison between the values of daytime AOC and the changes in the ozone concentration (Fig. 5a) suggests that the change in daytime AOC reflects primarily the changes in the net production rate of odd oxygen (Fig. S25-S24); this can be explained by the important role played by NO<sub>2</sub> in the wintertime formation of ozone.

#### 4. Summary and Policy Implications

The model simulations performed in the present study explore the response of radicals, of ozone, and of the atmospheric oxidative processes to a 50% reduction in primary emissions of key pollutants. Our analysis provides insight into the changes affecting ozone chemistry and the oxidizing processes to be expected in response to future emission reduction.

*In winter*, as most geographical areas are VOC-limited (saturated in NO<sub>x</sub>) a 50% reduction in NO<sub>x</sub> emissions leads to an ozone concentration increase of up to 8-10 ppbv (15-25%) in all geographical regions of China; this increase results from the reduced titration of ozone by nitric oxide. When combining this NO<sub>x</sub> reduction with a 50% reduction in AVOCs emissions, the ozone enhancement found in the rural areas and resulting from the reduced NO<sub>x</sub> is considerably reduced. However, in urban areas (VOC-limited situation), the ozone increase, although weakened, still exists (by 3.0-7.5 ppbv).

*In summer*, as most rural areas of China become NO<sub>x</sub>-limited, the geographical regions covered by the ozone increase in response to the 50% reduction applied to the NO<sub>x</sub> emissions shrink almost to the VOC-limited metropolitan areas. In these urban environments, the ozone increase

reaches a maximum of 10 ppbv or 17%. When the NO<sub>x</sub> emission reduction is combined with a 50% reduction in the VOC emissions, the increase in ozone almost disappears in all areas of China. This is explained by the significant decrease in ozone production resulting from the reduced level of hydrocarbons. However, in the areas where hydrocarbons are primarily of biological origin, the ozone concentration (i.e., linked to the photochemical degradation of isoprene) still slightly increases (i.e., by 0.5 ppbv or 1.3% at Guangzhou sites).

Formatted: Font color: Auto

*Paths to mitigation.* We conclude this paper by highlighting a few chemical paths that should be considered when designing a mitigation policy for a reduction of ozone in the urban areas of China. Figure 10 presents a schematic description of the chemical mechanisms involved in the chemical production of atmospheric ozone and highlights how different reaction paths tend to change the ozone abundance in response to a reduction in NO<sub>x</sub> and in anthropogenic VOC (AVOCs) emissions. This graph shows that a reduction in NO<sub>x</sub> emissions tends to increase the ozone concentration by (1) reducing the rate of the NO + O<sub>3</sub> reaction (ozone titration); (2) by increasing the rate of the HO<sub>2</sub> + NO reaction due to an increase in the HO<sub>2</sub> level associated with the reduced uptake of this radical by a lowered aerosol load; (3) by an increase in the atmospheric oxidizing capacity (AOC) through OH—and ozone-related reactions. The graph also shows that a decrease in AVOCs emissions tends (1) to reduce the level of the HO<sub>x</sub> radical and hence the ozone production by the HO<sub>2</sub> + NO reaction; (2) to enhance the level of OH radical—HO<sub>x</sub> due to the reduced aerosol uptake and (3) to reduce the AOC with a negative effect on the ozone concentration. The relative importance of these different chemical mechanisms varies with location and environmental conditions.

Formatted: Font color: Auto

We conclude that, in winter when the background ozone concentration is low, the reduction of NO<sub>x</sub> emissions tends to increase the level of near-surface ozone, while the reduction in AVOC emissions has the opposite effect. This conclusion applies both in rural and in urban areas. A combined reduction in the emissions of these two primary pollutants tends to decrease the level of ozone in rural areas, but to increase ozone in urban areas. Thus, in urban areas during winter, an effective approach to reduce the surface ozone concentration is through a strong limitation in the emissions of volatile organic compounds.

In summer when the ozone level is generally high, the reduction of NO<sub>x</sub> emissions is an effective action to reduce the ozone concentration in rural areas, but this measure is counterproductive in the NO<sub>x</sub>-saturated urban areas where ozone is controlled by VOCs. In fact, in urban areas during this season, the mechanisms involved in ozone mitigation are complex. For example, when NO<sub>x</sub> emissions are reduced, the atmospheric OH concentration is enhanced because of its reduced destruction by NO<sub>2</sub>. Following this increase in the OH concentration, an increase in the level of OVOCs, whose photolysis is an important source of HO<sub>x</sub> radicals, also leads to accelerated ozone production and further amplifies the oxidation of VOCs. In addition, the increase in AOC, linked to the reaction of OH and ozone with alkenes and the reactions of OH with OVOCs also contribute to an increase in the ozone production. Further, the reduction in the aerosol load resulting from a reduction in the emissions of aerosol precursors promotes the ozone formation by decreasing the aerosol extinction and by reducing the uptake of HO<sub>2</sub>. If combined with a 50% reduction in AVOCs, the increase in the OVOC

concentrations and in AOC, resulting from due to reduced NO<sub>x</sub> emissions, can be offset. However, the aerosol-related promotion of the level of OH and HO<sub>2</sub> radicals can be enhanced, highlighting the complexity of summertime ozone mitigation in urban areas.

910 ~~Table 2 provides quantitative information on the response of ozone at different urban locations~~  
~~for January and July.~~ In urban areas, the reduction in the level of surface ozone requires a  
915 reduction in the emissions of anthropogenic VOCs. However, for practical reasons, a 50%  
reduction in AVOCs emissions, as assumed in our study, is difficult to implement over a short  
period of time. With the known contribution of the VOCs-related reactions to the AOC, the  
reduction in the emissions of alkenes, aromatics, and unsaturated OVOCs, especially methanol  
and ethanol, should be a priority. The development of efficient mitigation strategies based on  
the reduction of AVOCs emissions requires, however, more detailed investigations on the  
920 reactivity of individual VOCs and on their potential impact on the ozone formation.

925  
930 **Code and data availability.** The WRF-Chem model is publicly available at  
<https://www2.mmm.ucar.edu/wrf/users/>. The modified code in the WRF-Chem model is  
available upon request to the corresponding author. The air quality data at surface stations are  
publicly available at the website of the Ministry of Ecology and Environment of the People's  
Republic of China at <http://english.mee.gov.cn/>.

935 **Author contributions.** JD and GB designed the structure of the manuscript, performed the  
numerical experiments, analyzed the results, and wrote the manuscript. JD analyzed the data  
and established the figures. All co-authors provided comments and reviewed the manuscript.

940 **Competing interests.** The authors declare that they have no conflict of interest.

945 **Acknowledgments.** The present joint Sino-German study was supported by the German  
Research Foundation (Deutsche Forschungs Gemeinschaft DFG), the National Science  
Foundation of China (NSFC) under Air-Changes grant no. 4487-20203, the Research Grants  
Council– University Grants Committee (grant no. T24-504/17-N) and the NSFC (grant  
no.42293322). The National Center for Atmospheric Research (NCAR) is sponsored by the  
US National Science Foundation. We would like to acknowledge the high-performance  
computing support from NCAR Cheyenne.

Formatted: Font color: Auto

Formatted: Font color: Auto

Formatted: Font color: Auto

Formatted: Font color: Auto

Formatted: Font color: Auto

Formatted: Font color: Auto

950

955

960

965

970

## References

975 China Air 2023, Air Pollution Prevention and Control Progress in Chinese Cities. <http://www.allaboutair.cn/uploads/231027/ChinaAir2023EN.pdf>

Dai, J., Brasseur, G. P., Vrekoussis, M., Kanakidou, M., Qu, K., Zhang, Y., Zhang, H., and Wang, T.: The atmospheric oxidizing capacity in China – Part I: Roles of different photochemical processes, *Atmos. Chem. Phys.*, 23, 14127–14158, <https://doi.org/10.5194/acp-23-14127-2023>, 2023.

985 Emmons, L. K., Walters, S., Hess, P. G., Lamarque, J.-F., Pfister, G. G., Fillmore, D., Granier, C., Guenther, A., Kinnison, D., Laepple, T., Orlando, J., Tie, X., Tyndall, G., Wiedinmyer, C., Baughcum, S. L., and Kloster, S.: Description and evaluation of the Model for Ozone and Related chemical Tracers, version 4 (MOZART-4), *Geosci. Model Dev.*, 3, 43–67, <https://doi.org/10.5194/gmd-3-43-2010>, 2010.

990 Jacob, D. J., Horowitz, L. W., Munger, J. W., Heikes, B. G., Dickerson, R. R., Artz, R. S., and Keene, W. C.: Seasonal transition from NO<sub>x</sub> - to hydrocarbon-limited conditions for ozone production over the eastern United States in September, *J. Geophys. Res.-Atmo.*, 100, 9315–9324, <https://doi.org/10.1029/94JD03125>, 1995.

- 995 Knote, C., Hodzic, A., Jimenez, J. L., Volkamer, R., Orlando, J. J., Baidar, S., Brioude, J., Fast, J., Gentner, D. R., Goldstein, A. H., Hayes, P. L., Knighton, W. B., Oetjen, H., Setyan, A., Stark, H., Thalman, R., Tyndall, G., Washenfelder, R., Waxman, E., and Zhang, Q.: Simulation of semi-explicit mechanisms of SOA formation from glyoxal in aerosol in a 3-D model, *Atmos. Chem. Phys.*, 14, 6213–6239, <https://doi.org/10.5194/acp-14-6213-2014>, 2014.
- 1000 Li, B., Ho, S.S.H., Li, X., Guo, L., Chen, A., Hu, L., Yang, Y., Chen, D., Lin, A., Fang, X., A comprehensive review on anthropogenic volatile organic compounds (VOCs) emission estimates in China: comparison and outlook. *Environ. Int.* 156, 106710, <https://doi.org/10.1016/j.envint.2021.106710>, 2021.
- 1005 Li, C., Liu, Y., Cheng, B., Zhang, Y., Liu, X., Qu, Y., Feng, M.: A comprehensive investigation on volatile organic compounds (VOCs) in 2018 in Beijing, China: Characteristics, sources and behaviors in response to O<sub>3</sub> formation. *Sci. Total Environ.* 806, 150247, <https://doi.org/10.1016/j.scitotenv.2021.150247>, 2022.
- 1010 Li, J., Xie, X., Li, L., Wang, X., Wang, H., Jing, S. A., Hu, J.: Fate of Oxygenated Volatile Organic Compounds in the Yangtze River Delta Region: Source Contributions and Impacts on the Atmospheric Oxidation Capacity. *Environ. Sci., Technol.*, 56(16), 11212–11224, <https://doi.org/10.1021/acs.est.2c00038>, 2022.
- 1015 Li, K., Jacob, D. J., Liao, H., Shen, L., Zhang, Q., Bates, K. H.: Anthropogenic drivers of 2013–2017 trends in summer surface ozone in China. *Proc. Natl. Acad. Sci.*, 116 (2), 422–427, <https://doi.org/10.1073/pnas.1812168116>, 2019.
- 1020 Li, K., Jacob, D. J., Liao, H., Qiu, Y., Shen, L., Zhai, S., Kuk, S. K.: Ozone pollution in the North China Plain spreading into the late-winter haze season. *Proc. Natl. Acad. Sci.*, 118(10), e2015797118, <https://doi.org/10.1073/pnas.2015797118>, 2021.
- 1025 Liu, T., Hong, Y., Li, M., Xu, L., Chen, J., Bian, Y., Yang, C., Dan, Y., Zhang, Y., Xue, L., Zhao, M., Huang, Z., and Wang, H.: Atmospheric oxidation capacity and ozone pollution mechanism in a coastal city of southeastern China: analysis of a typical photochemical episode by an observation-based model, *Atmos. Chem. Phys.*, 22, 2173–2190, <https://doi.org/10.5194/acp-22-2173-2022>, 2022.
- 1030 Liu, Y., Geng, G., Cheng, J., Liu, Y., Xiao, Q., Liu, L., Zhang, Q.: Drivers of Increasing Ozone during the Two Phases of Clean Air Actions in China 2013–2020. *Environ. Sci., Technol.*, <https://doi.org/10.1021/acs.est.3c00054>, 2023
- 1035 Liu, Y., and Wang Tao: Worsening urban ozone pollution in China from 2013 to 2017 – Part 2: The effects of emission changes and implications for multi-pollutant control, *Atmos. Chem. Phys.*, 20, 6323–6337, <https://doi.org/10.5194/acp-206323>, 2020.

Formatted: Font color: Auto

Formatted: Font color: Auto

Formatted: Font color: Auto

Formatted: Font color: Auto

Formatted: Font color: Auto

Formatted: Font color: Auto

Formatted: Font color: Auto

Formatted: Font color: Auto

Formatted: Font color: Auto

Formatted: Font color: Auto

Formatted: Font color: Auto

Formatted: Font color: Auto

Formatted: Font color: Auto

Formatted: Font color: Auto

Formatted: Font color: Auto

Formatted: Font color: Auto

Formatted: Font color: Auto

Formatted: Font color: Auto



1040 Meng, F., Zhang, Y., Kang, J., Heal, M. R., Reis, S., Wang, M., Liu, L., Wang, K., Yu, S., Li,  
P., Wei, J., Hou, Y., Zhang, Y., Liu, X., Cui, Z., Xu, W., and Zhang, F.: Trends in secondary  
inorganic aerosol pollution in China and its responses to emission controls of precursors in  
wintertime, *Atmos. Chem. Phys.*, 22, 6291–6308, <https://doi.org/10.5194/acp-22-6291-2022>,  
2022.

1045 Ou, J., Yuan, Z., Zheng, J., Huang, Z., Shao, M., Li, Z., Louie, P. K.: Ambient ozone control  
in a photochemically active region: short-term despiking or long-term attainment? *Environ.  
Sci., Technol.*, 50 (11), 5720-5728, <https://doi.org/10.1021/acs.est.6b00345>, 2016.

1050 Skamarock, W.C., Klemp, J.B., Dudhia, J., Gill, D.O., Liu, Z., Berner, J., Wang, W., Powers,  
J.G., Duda, M.G., Barker, D.M.: A Description of the Advanced Research WRF Model Version  
4; Mesoscale and Microscale Meteorology Laboratory NCAR: Boulder, CO, USA, 2019.

1055 Song, H., Lu, K., Dong, H., Tan, Z., Chen, S., Zeng, L., Zhang, Y.: Reduced aerosol uptake  
of hydroperoxyl radical may increase the sensitivity of ozone production to volatile organic  
compounds. *Environ. Sci., Technol. Lett.*, 9(1), 22-29.  
<https://doi.org/10.1021/acs.estlett.1c00893>, 2021.

1060 Tan, Z., Lu, K., Hofzumahaus, A., Fuchs, H., Bohn, B., Holland, F., Liu, Y., Rohrer, F., Shao,  
M., Sun, K., Wu, Y., Zeng, L., Zhang, Y., Zou, Q., Kiendler-Scharr, A., Wahner, A., and  
Zhang, Y.: Experimental budgets of OH, HO<sub>2</sub>, and RO<sub>2</sub> radicals and implications for ozone  
formation in the Pearl River Delta in China 2014, *Atmos. Chem. Phys.*, 19, 7129–7150,  
<https://doi.org/10.5194/acp-19-7129-2019>, 2019.

1065 Tan, Z., Lu, K., Ma, X., Chen, S., He, L., Huang, X., Zhang, Y.: Multiple Impacts of Aerosols  
on O<sub>3</sub> Production Are Largely Compensated: A Case Study Shenzhen, China. *Environ. Sci.,  
Technol.*, 56(24), 17569-17580, <https://doi.org/10.1021/acs.est.2c06217>, 2022.

1070 Tonnesen, G. S., and R. L. Dennis.: Analysis of radical propagation efficiency to assess ozone  
sensitivity to hydrocarbons and NO<sub>x</sub>: 2. Long-lived species as indicators of ozone  
concentration sensitivity, *J. Geophys. Res.*, 105(D7), 9227–9241,  
<https://doi.org/10.1029/1999JD900372>, 2000.

1075 Wang, J, Zhang Y, Xiao S, Wu Z, Wang X.: Ozone Formation at a Suburban Site in the Pearl  
River Delta Region, China: Role of Biogenic Volatile Organic Compounds. *Atmosphere*, 14  
(4):609. <https://doi.org/10.3390/atmos14040609>, 2023.

1075 Wang, T., Xue, L., Feng, Z., Dai, J., Zhang, Y., Tan, Y.: Ground-level ozone pollution in  
China: a synthesis of recent findings on influencing factors and impacts. *Environ. Res. Letters*,  
17(6), 063003. <https://doi.org/10.1088/1748-9326/ac69fe>, 2022.

Formatted: Font color: Auto

Formatted: Font color: Auto

Formatted: Font color: Auto

Formatted: Font color: Auto

Formatted: Font color: Auto

Formatted: Font color: Auto

Formatted: Font color: Auto

Formatted: Font color: Auto

Formatted: Font color: Auto

Formatted: Font color: Auto

Formatted: Font color: Auto

Formatted: Font color: Auto

Formatted: Font color: Auto

Formatted: Font color: Auto

Formatted: Font color: Auto

Formatted: Font color: Auto

Formatted: Font color: Auto

Formatted: Font color: Auto

Formatted: Font color: Auto

1080 Wang, W., van der A, R., Ding, J., van Weele, M., and Cheng, T.: Spatial and temporal changes  
of the ozone sensitivity in China based on satellite and ground-based observations, *Atmos.*  
*Chem. Phys.*, 21, 7253–7269, <https://doi.org/10.5194/acp-21-7253-2021>, 2021.

1085 Wang, W., Yuan, B., Peng, Y., Su, H., Cheng, Y., Yang, S., Wu, C., Qi, J., Bao, F., Huangfu,  
Y., Wang, C., Ye, C., Wang, Z., Wang, B., Wang, X., Song, W., Hu, W., Cheng, P., Zhu, M.,  
Zheng, J., and Shao, M.: Direct observations indicate photodegradable oxygenated volatile  
organic compounds (OVOCs) as larger contributors to radicals and ozone production in the  
atmosphere, *Atmos. Chem. Phys.*, 22, 4117–4128, <https://doi.org/10.5194/acp-22-4117-2022>,  
2022.

1090 Xue, L., Gu, R., Wang, T., Wang, X., Saunders, S., Blake, D., Louie, P. K. K., Luk, C. W. Y.,  
Simpson, I., Xu, Z., Wang, Z., Gao, Y., Lee, S., Mellouki, A., and Wang, W.: Oxidative  
capacity and radical chemistry in the polluted atmosphere of Hong Kong and Pearl River Delta  
region: analysis of a severe photochemical smog episode, *Atmos. Chem. Phys.*, 16, 9891–9903,  
<https://doi.org/10.5194/acp-16-9891-2016>, 2016.

1095 Yang, G., Liu, Y., Li, X. Spatiotemporal distribution of ground-level ozone in China at a city  
level. *Sci Rep* 10, 7229, <https://doi.org/10.1038/s41598-020-64111-3>, 2020.

1100 Zaveri, R. A., R. C. Easter, J. D. Fast, and L. K. Peters, Model for Simulating Aerosol  
Interactions and Chemistry (MOSAIC), *J. Geophys. Res.*, 113, D13204,  
[doi:10.1029/2007JD008782](https://doi.org/10.1029/2007JD008782), 2008

1105 Zhang, Y., Dai, J., Li, Q., Chen, T., Mu, J., Brasseur, G., Wang, T., Xue, L.: Biogenic volatile  
organic compounds enhance ozone production and complicate control efforts: Insights from  
long-term observations in Hong Kong. *Atmos. Environ.*, 309, 119917,  
<https://doi.org/10.1016/j.atmosenv.2023.119917>, 2023.

1110 Zhao, X., Zhou, W., and Han, L.: Human activities and urban air pollution in Chinese mega  
city: An insight of ozone weekend effect in Beijing, *Phys Chem Earth Pt. A/B/C*, 110, 109–  
116, <https://doi.org/10.1016/j.pce.2018.11.005>, 2019.

1115 Zheng, B., Tong, D., Li, M., Liu, F., Hong, C., Geng, G., Li, H., Li, X., Peng, L., Qi, J., Yan,  
L., Zhang, Y., Zhao, H., Zheng, Y., He, K., and Zhang, Q.: Trends in China's anthropogenic  
emissions since 2010 as the consequence of clean air actions, *Atmos. Chem. Phys.*, 18, 14095–  
14111, <https://doi.org/10.5194/acp-18-14095-2018>, 2018

1120 Zhu, S., Ma, J., Wang, S., Sun, S., Wang, P., Zhang, H.: Shifts of formation regimes and  
increases of atmospheric oxidation led to ozone increase in North China Plain and Yangtze  
River Delta from 2016 to 2019. *J. Geophys. Res.: Atmos.*, e2022JD038373,  
<https://doi.org/10.1029/2022JD038373>, 2023.

Formatted: Font color: Auto

Formatted: Font color: Auto

Formatted: Font color: Auto

1125  
1130  
1135  
1140  
1145  
1150  
1155

Table 1. Sensitivity experiments

Model Experiments	Description
<i>BASE</i>	Without emission reduction
<i>NOx</i>	With emission reduction in NO <sub>x</sub> <sup>a</sup> by a factor of 2
<i>AVOCs</i>	With emission reduction in anthropogenic VOCs <sup>a</sup> by a factor of 2

Formatted: Font color: Auto

Formatted: Font color: Auto

Formatted: Font color: Auto

1160  
1165  
1170  
1175  
1180  
1185  
1190

*N+A* With emission reduction  
in  $\text{NO}_x^a$  and anthropogenic VOCs<sup>a</sup> by a factor of 2

*TOTAL* With emission reduction in all species<sup>a</sup>  
by a factor of 2

Formatted: Font color: Auto

Formatted: Font color: Auto

Formatted: Font color: Auto

<sup>a</sup> Relevant species is shown in Sect. 2.1 and Table S1 in Supplementary Materials.

Table 2. Ozone changes due to reduction in emissions (in percentage)

Location	Sites name	Ozone changes in winter condition (Mean ± SD)			
		$\text{NO}_x^a$	$\text{AVOCs}^b$	$N+A^c$	$TOTAL^d$
North	Beijing	25.0 ± 25.2 <sup>e</sup>	-2.5 ± 1.3	22.0 ± 32.8	20.0 ± 19.5
East	Shanghai	33.2 ± 35.3	-18.2 ± 13.5	21.8 ± 20.5	22.7 ± 18.8
South	Guangzhou	21.4 ± 22.6	-17.1 ± 11.2	7.1 ± 3.2	10.0 ± 3.5

Location	Sites name	Ozone changes in summer condition (Mean ± SD)			
		<i>NO<sub>x</sub></i>	<i>AVOCs</i>	<i>N+A</i>	<i>TOTAL</i>
West	Chengdu	21.3 ± 23.8	-9.4 ± 8.5	14.1 ± 8.3	20.3 ± 13.5
North	Beijing	6.4 ± 3.8	-21.8 ± 19.2	-5.5 ± 4.2	-7.3 ± 5.0
East	Shanghai	17.1 ± 12.8	-22.9 ± 20.8	-2.9 ± 2.1	-2.6 ± 1.5
South	Guangzhou	15.0 ± 13.1	-14.5 ± 13.5	1.3 ± 1.0	1.3 ± 0.9
West	Chengdu	5.5 ± 4.5	-14.5 ± 10.2	-5.5 ± 2.0	-4.5 ± 1.9

a-d. Sensitivity cases with a 50% reduction in the emissions of  $\text{NO}_x$  (*NO<sub>x</sub>*), *AVOCs* (*AVOCs*),  $\text{NO}_x$  and *AVOCs* (*N+A*), and other species ( $\text{NO}_x$ , *AVOCs*,  $\text{CO}$ ,  $\text{NH}_3$ ,  $\text{SO}_2$ ) under consideration (*TOTAL*).

e. Values are displayed in the average ozone changes during daytime (06:00-19:00) in percentage with the standard deviation as the error bar. (ozone changes = (case value – base value)/base value × 100).

Formatted: Font color: Auto

1195  
1200  
1205  
1210  
1215  
1220  
1225  
1230

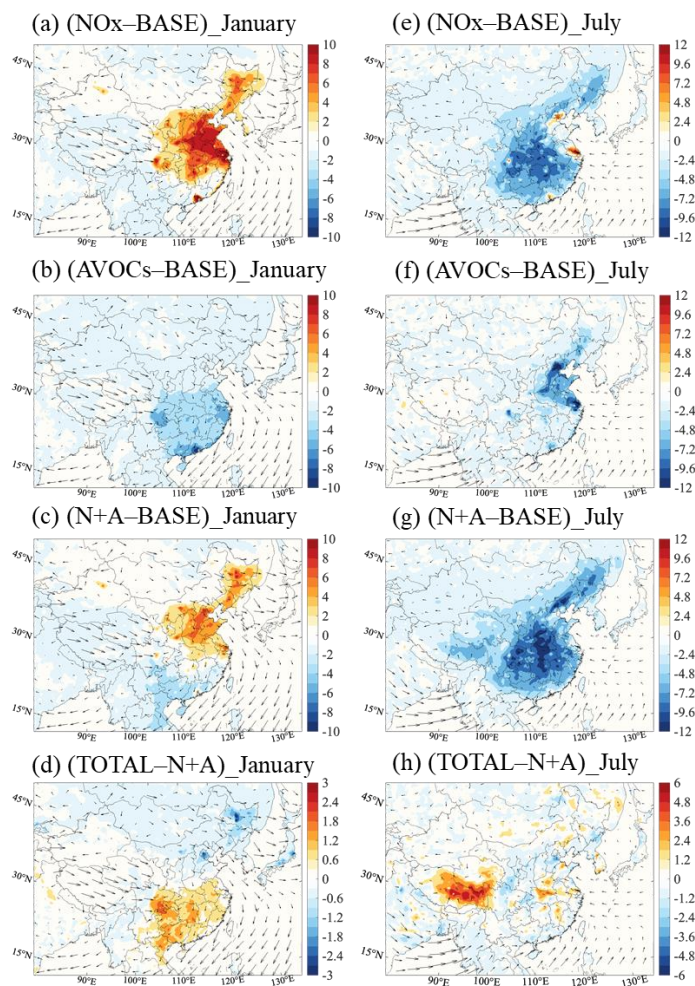


Figure 1. Changes in the monthly-averaged daytime (06:00 to 19:00 LST) surface ozone concentration (Unit: ppbv) response to a 50% reduction in  $\text{NO}_x$  emissions (a, e; *NO<sub>x</sub>* case), in anthropogenic VOCs (AVOCs) emissions (b, f; *AVOCs* case) and in combined  $\text{NO}_x$  and AVOCs emissions (c, g; *N+A* case) relative to *BASE* case and to the additional reduction in the emission of  $\text{CO}$ ,  $\text{NH}_3$  and  $\text{SO}_2$  by 50% (d, h; *TOTAL* case) relative to *N+A* case for January (a-d) and July (e-h) 2018. Arrows represent the wind speed and wind direction. Notice the inconsistency in the scale of Figure 1d and 1h.

Formatted: Font color: Auto

Formatted: Font color: Auto

Formatted: Centered

Formatted: Font color: Auto, Subscript

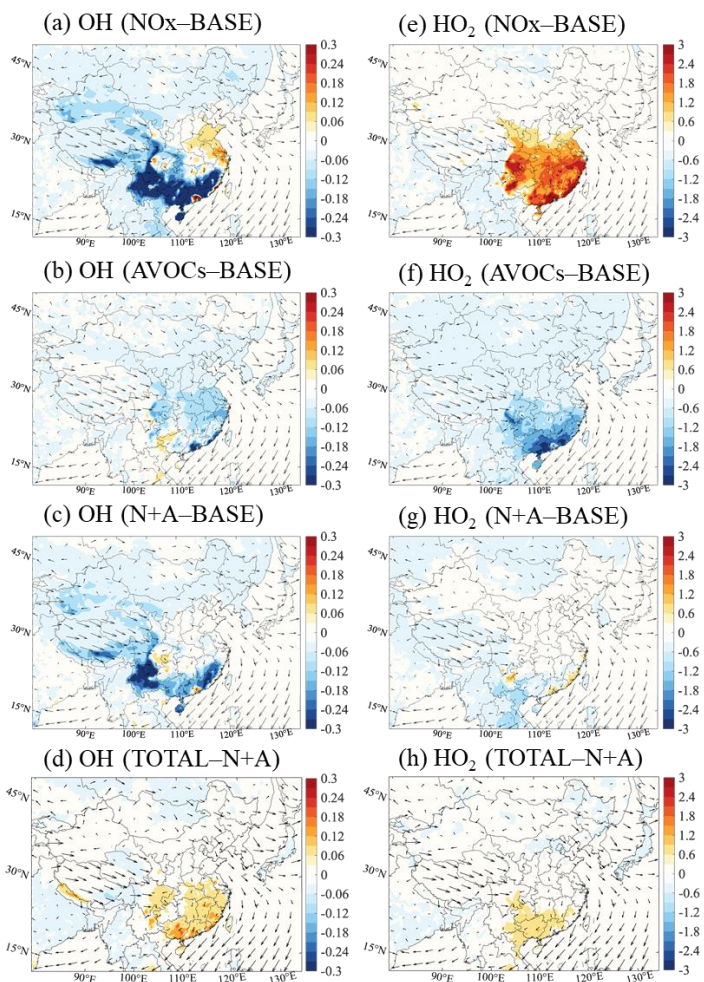
Formatted: Font color: Auto

Formatted: Font color: Auto, Subscript

Formatted: Font color: Auto

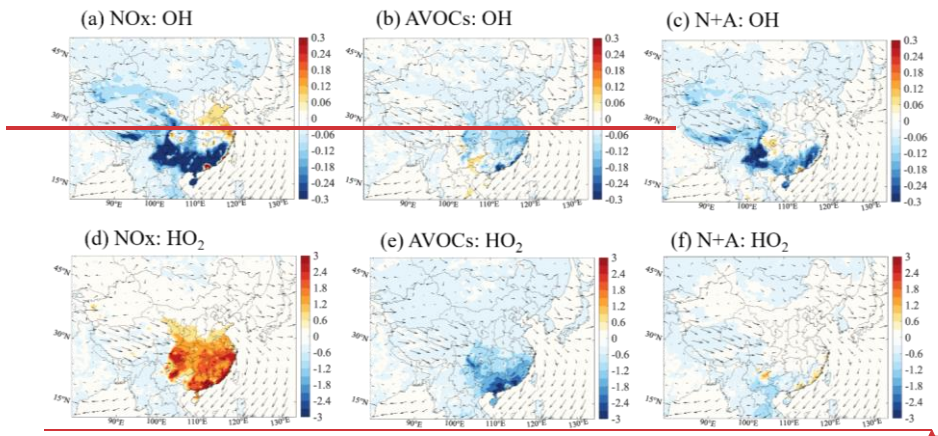
Formatted: Font: Italic, Font color: Auto

Formatted: Font color: Auto



Formatted: Font color: Auto





1245 Figure 42. Changes in the monthly-averaged daytime (06:00 to 19:00 LST) surface mixing  
 1250 ratio of OH radical (a-e*d*, Unit: 0.1 pptv) and HO<sub>2</sub> radical (e*e*-f*h*, Unit: pptv) response to a 50%  
 reduction in the emissions of NO<sub>x</sub> (a, e*e*; *NOx* case), anthropogenic VOCs (b, e*f*; *AVOCs* case)  
 and in NO<sub>x</sub> and AVOCs (c, f*g*; *N+A* case) relative to *BASE* case and in additional emission  
reduction of other species (d, h; *TOTAL* case) relative to *N+A* case for January of 2018. Arrows

Formatted: Font color: Auto

Formatted: Font: Italic, Font color: Auto

Formatted: Font color: Auto

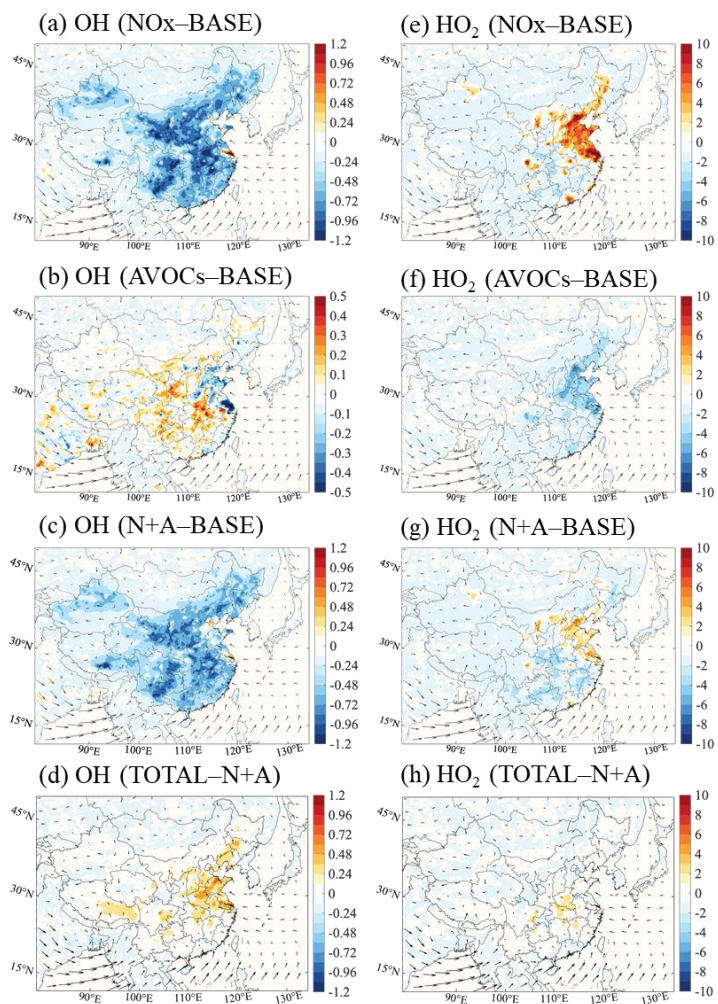
Formatted: Font: Italic, Font color: Auto

Formatted: Font color: Auto

1255

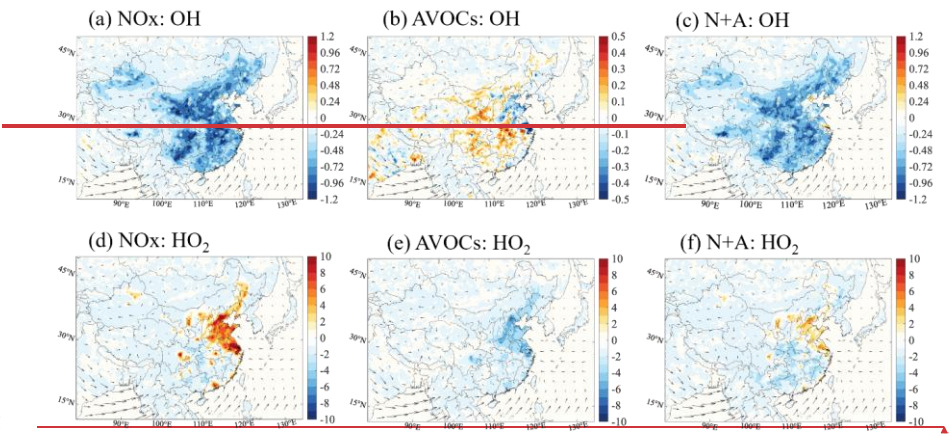
1260





Formatted: Font color: Auto

Formatted: Font color: Auto



1265

Figure 23. Same as Fig. 22 but for July of 2018. Notice the inconsistency in the scale of Figure 2b.

1270

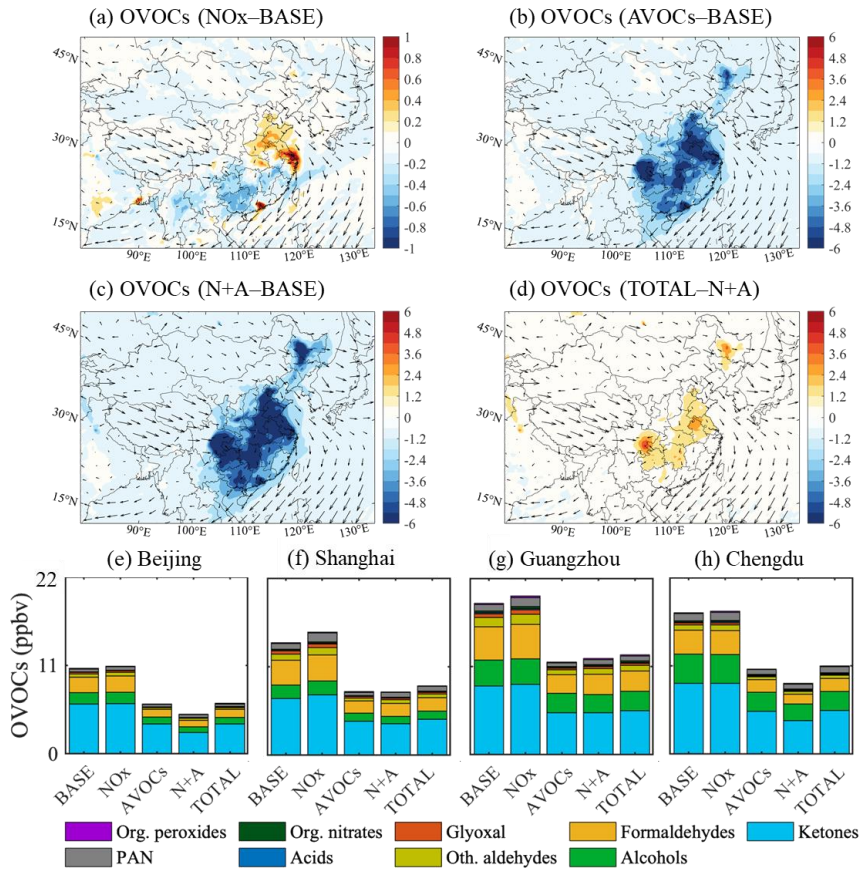


Figure 34. Changes in the monthly-averaged surface concentration of total oxidized VOCs (OVOCs) for January 2018. (a-d) Changes in the concentration of total OVOCs (Unit: ppbv) response to the reduction in  $NO_x$ ,  $AVOCs$  and combined  $NO_x$  and  $AVOCs$  emissions ( $N+A$ ) relative to the  $BASE$  case and to the reduction in the total emission of considered species ( $TOTAL$ ) relative to the  $N+A$  case. (e-h) Averaged concentration of OVOC contributed by different species at four city sites (Beijing, Shanghai, Guangzhou, and Chengdu) in China in five simulated cases ( $BASE$ ,  $NO_x$ ,  $AVOCs$ ,  $N+A$ , and  $TOTAL$  cases). Arrows in a-c represent the wind speed and wind direction. Notice the inconsistency in the scale of Figure 3a.

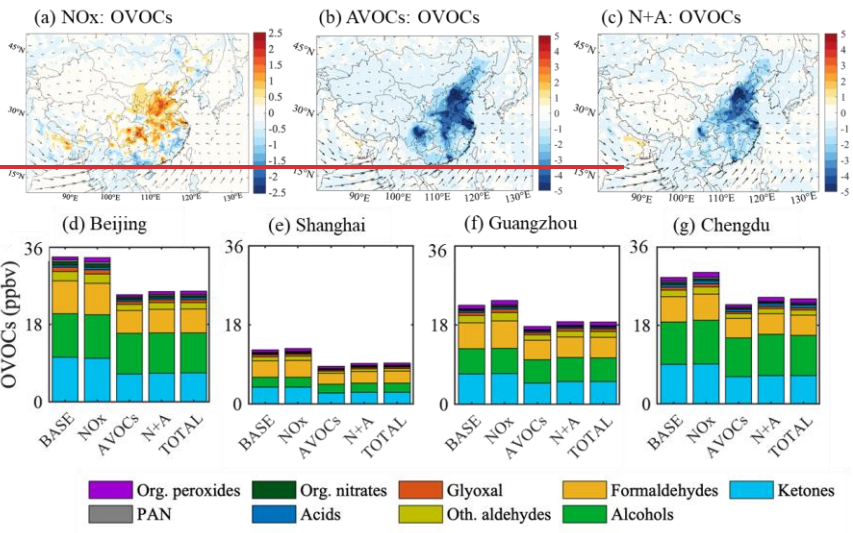
Formatted: Font color: Auto

Formatted: Font color: Auto

1275

1280

1285



Formatted: Font color: Auto

Formatted: Font color: Auto

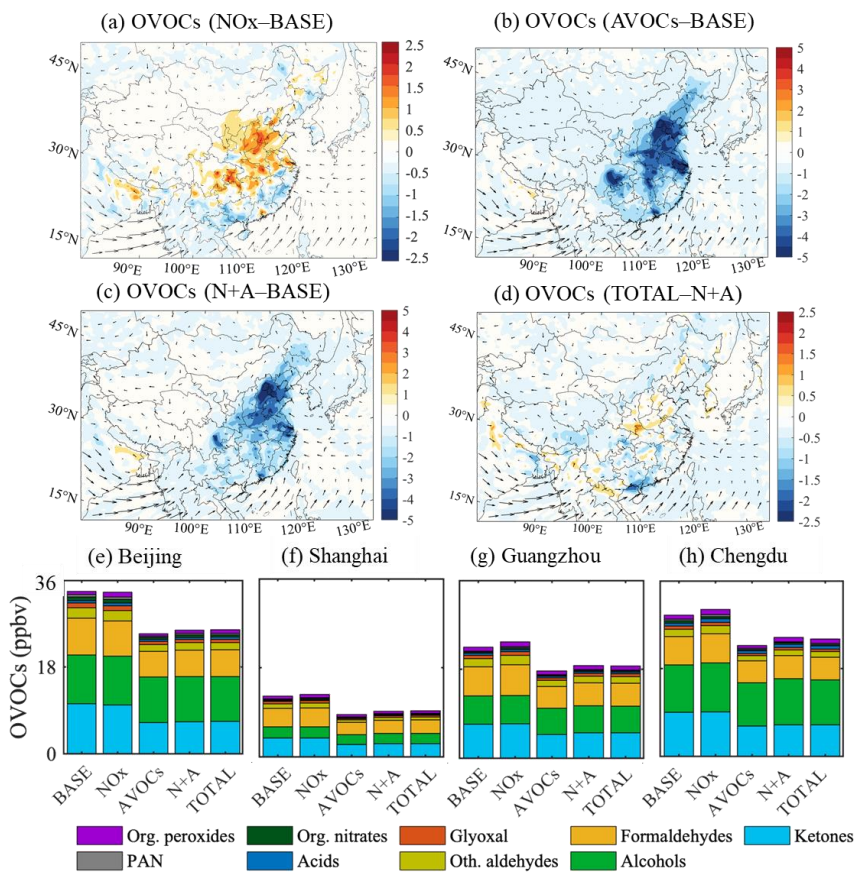


Figure 45. Same as Fig. 3-4 but for July of 2018. Notice the inconsistency in the scale of Figure 4 a, d with Figure 4 b, c.

Formatted: Font color: Auto

Formatted: Font color: Auto

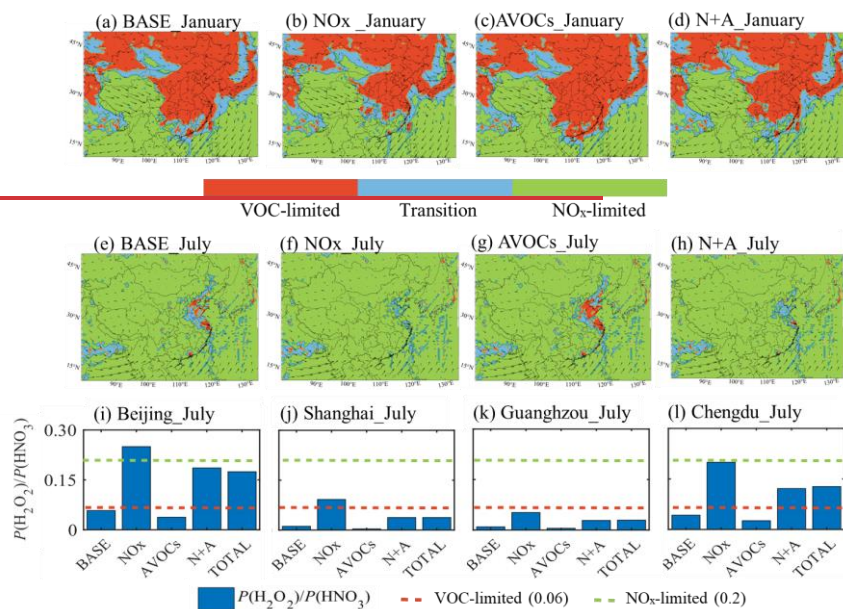
1290

1295

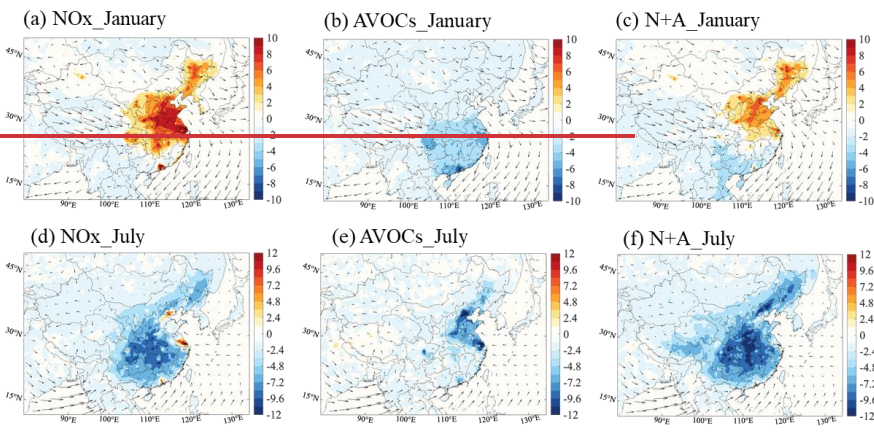
1300

1305



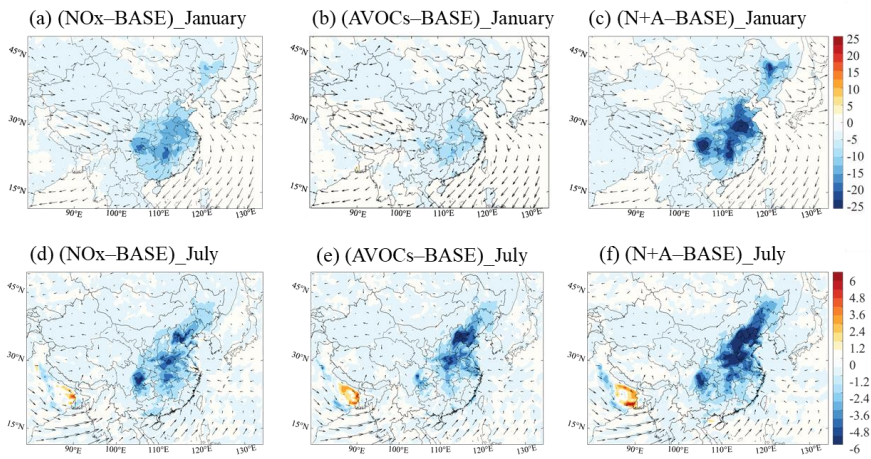


1310 Figure 5. Ozone sensitivity regimes and their changes due to emission reduction. (a-h) Display  
 1315 of regions in which ozone production is limited by the availability of nitrogen oxides (NO<sub>x</sub>-  
 limited, in green), and volatile organic components (VOC limited, in red) under the emissions  
 in case of *BASE*, *NO<sub>x</sub>*, *AVOCs*, and *N+A* conditions in January (a-d) and July (e-h) of 2018.  
 The regions where ozone production is controlled by the availability of both NO<sub>x</sub> and VOCs  
 (transition) are shown in blue. (i-l) The daytime (06:00 to 19:00 LST) value of the ratio between  
 the production rate of hydrogen peroxide (H<sub>2</sub>O<sub>2</sub>) and nitric acid (HNO<sub>3</sub>) [ $P(\text{H}_2\text{O}_2)/P(\text{HNO}_3)$ ]  
 at four city sites (Beijing, Shanghai, Chengdu, Guangzhou) in China in the five simulated cases  
 for July 2018.

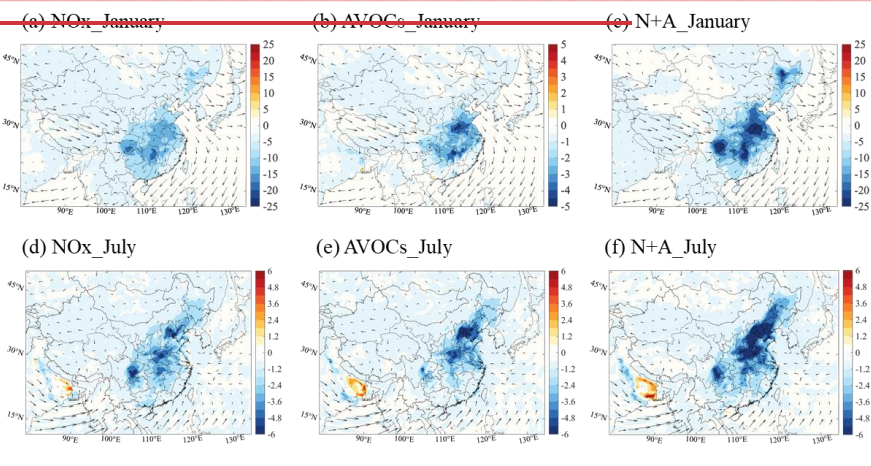


1320  
1325  
1330  
1335  
1340

Figure 6. Changes in the monthly averaged daytime surface ozone concentration (Unit: pptv) response to a 50% reduction in NO<sub>x</sub> emissions (*NO<sub>x</sub> case*), in anthropogenic VOCs (*AVOCs case*) and in combined NO<sub>x</sub> and AVOCs emissions (*N+A case*) relative to *BASE* case for January (a-c) and July (d-f) 2018. Arrows represent the wind speed and wind direction.



Formatted: Font color: Auto



Formatted: Font color: Auto

1345

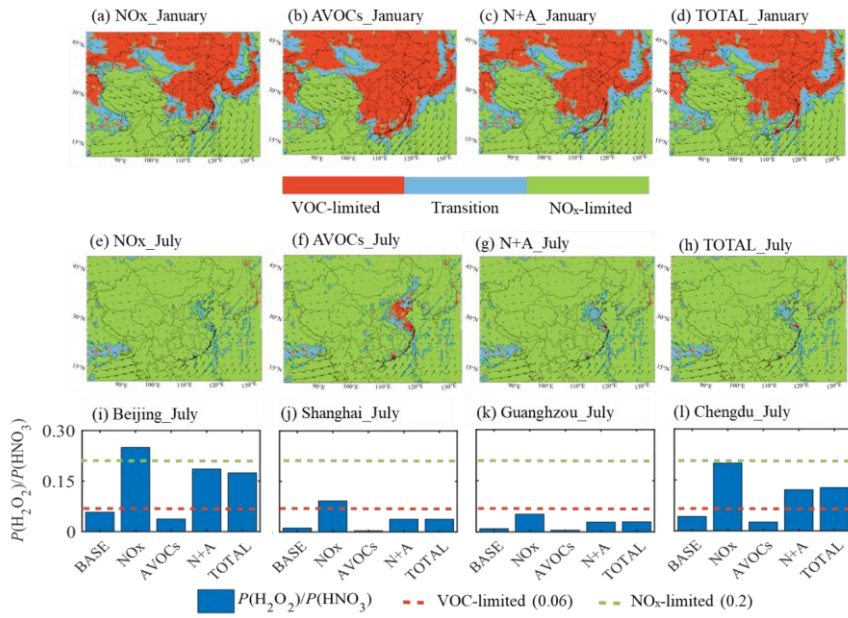
Figure 76. Changes in the monthly-averaged surface concentration of fine particulate aerosol (Unit:  $\mu\text{g m}^{-3}$ ) in response to  $\text{NO}_x$  (a, d), AVOCs (b, e) and N+A case (c, f) relative to BASE case for January (a-c) and July (d-f) 2018. Arrows represent the wind speed and wind direction. Notice the inconsistency in the scale of Figure 7b.

1350

1355



1360



Formatted: Font color: Auto

Formatted: Font color: Auto

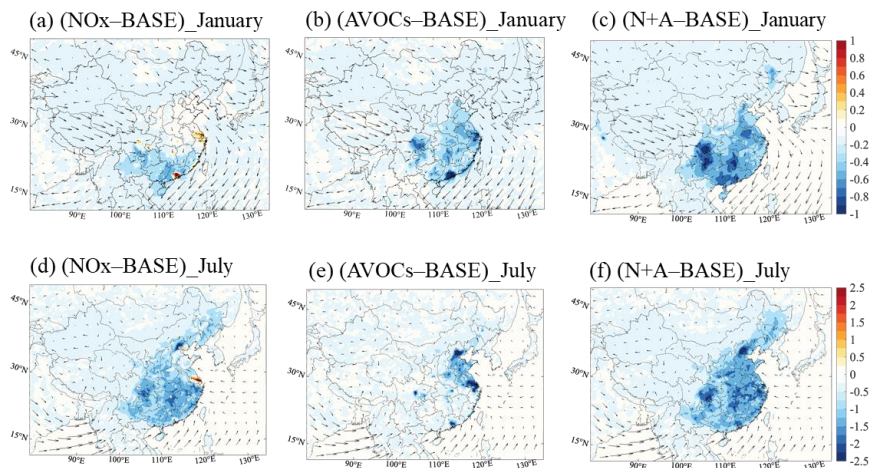
1365

Figure 7. Impact of the emission reduction on ozone sensitivity regimes. (a-h) Display of ozone sensitivity regions in which ozone production is limited by the availability of nitrogen oxides (NO<sub>x</sub>-limited, in green), and volatile organic components (VOC-limited, in red) under the emissions in case of NO<sub>x</sub>, AVOCs, N+A, and TOTAL conditions in January (a-d) and July (e-h) of 2018. The regions where ozone production is controlled by the availability of both NO<sub>x</sub> and VOCs (transition) are shown in blue. (i-l) The daytime (06:00 to 19:00 LST) value of the ratio between the production rate of hydrogen peroxide (H<sub>2</sub>O<sub>2</sub>) and nitric acid (HNO<sub>3</sub>) [ $P(H_2O_2)/P(HNO_3)$ ] at four city sites (Beijing, Shanghai, Chengdu, Guangzhou) in China in the five simulated cases for July 2018.

1370

Formatted: Font color: Auto

1375



1380

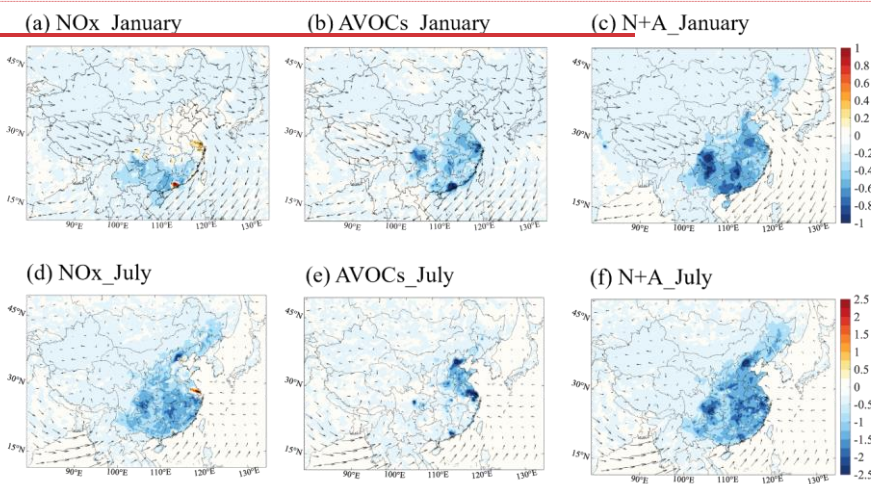


Figure 8. Changes in the monthly-averaged daytime value of atmospheric oxidizing capacity (AOC, Unit:  $10^7$  molec.  $\text{cm}^{-3}$   $\text{s}^{-1}$ ) response to  $\text{NO}_x$  (a, d), AVOCs (b, e), and  $\text{N}+\text{A}$  (c, f) cases relative to *BASE* case for January (a-c) and July (d-f) 2018.

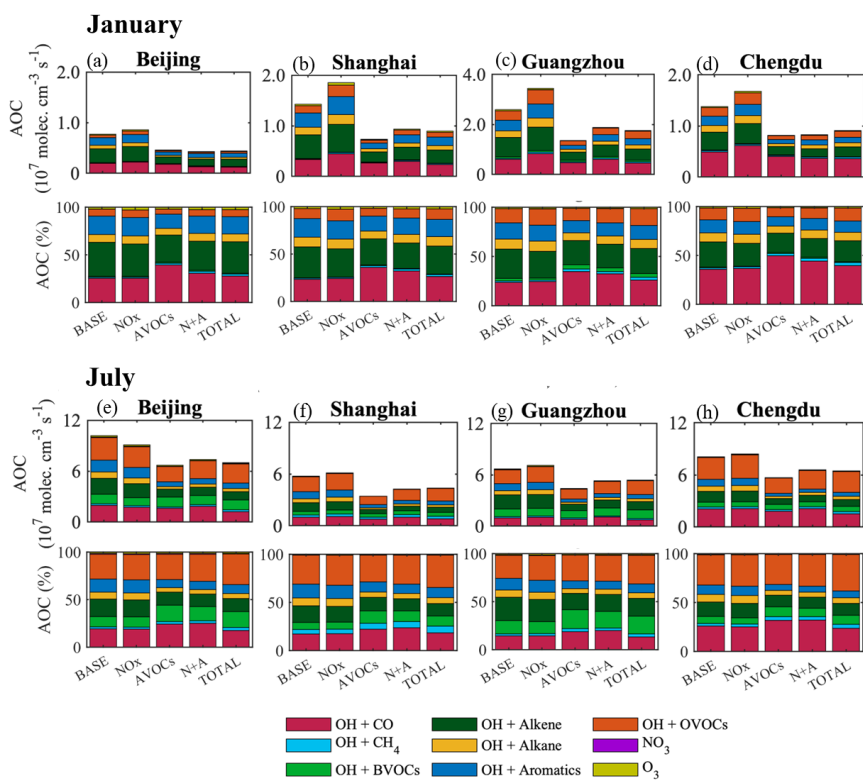
1385

1390

Formatted: Font color: Auto

Formatted: Font color: Auto

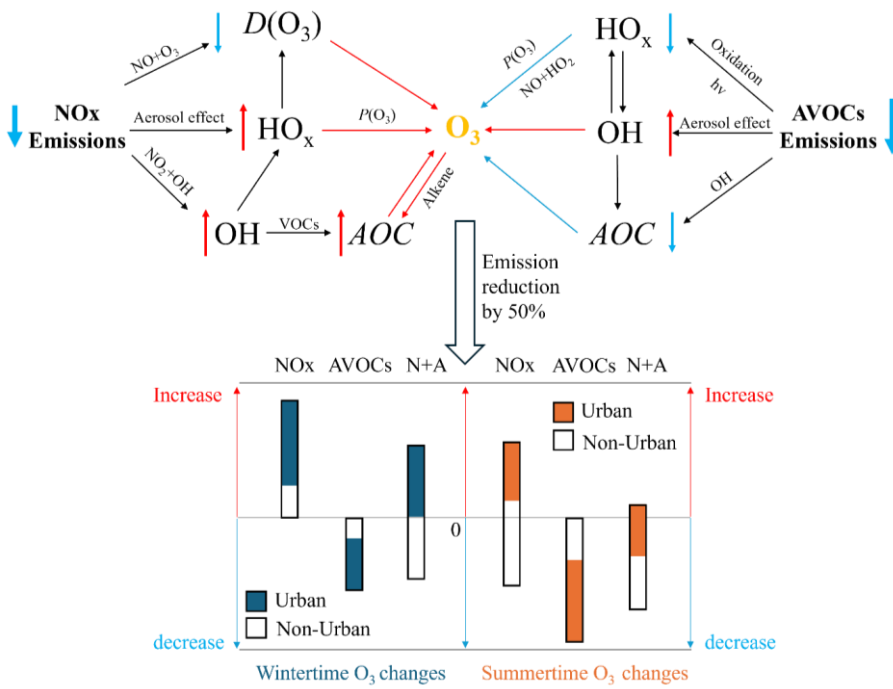
Formatted: Font color: Auto



1395 Figure 9. Monthly-averaged value (Unit:  $10^7$  molec.  $\text{cm}^{-3} \text{s}^{-1}$ ) and relative terms (Unit: %) of  
 1400 daytime AOC at the sites of Beijing (a, e), Shanghai (b, f), Guangzhou (c, g), and Chengdu (d,  
 1405 h) in five simulated cases (*BASE*, *NO<sub>x</sub>*, *AVOCs*, *N+A*, *TOTAL* cases) in January (a-d) and July  
 1410 (e-h) of 2018. Notice the inconsistency in the scale of Figure 9c.

1400  
1405  
1410  
1415

Formatted: Font color: Auto  
Formatted: Font color: Auto



1420 Figure 10. Schematics show the responses of oxidative processes, associated with ozone  
 1425 formation, to the reduction in primary emissions of  $NO_x$  and AVOCs in urban areas (VOC-  
 limited) in winter and summer. Arrows besides the chemicals represent the changes associated  
 with the reduction in emission. (decrease trend shown in blue; increase trend shown in red)  
 Blue and red arrows closing to  $O_3$  represent the positive and negative contributions to the ozone  
 1430 formations.  $AOC$ ,  $P(O_3)$ , and  $D(O_3)$  are the abbreviations of the Atmospheric Oxidative  
 Capacity, production of ozone, and destruction of ozone. Bar figure shows the ranges of ozone  
 changes in whole of China (black bar), in non-urban areas (white part in the bar), and in urban  
 areas (colored part in the bar) in three emissions cases ( $NO_x$ ,  $AVOCs$ , and  $N+A$  represent the  
 case with emission reduction in  $NO_x$ , Anthropogenic VOCs (AVOCs), and the combined  $NO_x$   
 and AVOCs emissions, respectively) relative to *BASE* cases in winter and summer conditions.